CHAPTER III

ELECTRICAL STUDIES IN MOLYBDENUM TRIOXIDE, VANADIUM PENTOXIDE, AND TITANIUM DIOXIDE FILMS.

3.1. Introduction.

The electrical conduction in thin film of transition metal oxides depends upon temperature, structure and thickness. DC conductivity of the transition metal oxide films in a coplanar geometry ($\sigma_{\parallel}$) and in a sandwich geometry ($\sigma_{\perp}$) have been investigated. Capacitance of the MIMs have been studied for the transition metal oxide viz., MoO_3, V_2O_5, and TiO_2. Transition metal oxides have been extensively studied since the discovery of their semiconducting properties[1].

The transition metal oxides form predominantly ionic solids which exhibits a wide range of electrical and optical properties. The 4d oxides such as MoO_3 are expected to be more ionic than the 3d oxides because the 4d electrons are less tightly bonded to metal atoms than 3d electrons. With increased ionicity, the oxides tend to deviate from stoichiometry, and the non-stoichiometry is associated with modification of electrical properties and colour centre formation[2]. The energy associated with the anion defects of MoO_{3-x} must be greater than k_BT at ambient temperature in order to trap the electrons. MoO_3 forms a series of non-stoichiometric

oxides in a reducing atmosphere and can produce blue colouration. The colouration in MoO_3 is largely due to electrons trapped in anion vacancies[3]. MoO_3 has a very interesting orthorhombic layer structure, consisting of zig-zag rows of MoO_6 octahedra which share edge, while the rows are mutually connected by corners[4]. Compounds having layer structure show considerable interesting electrical properties. MoO_3 appears to be a material intermediate between insulators and semiconductors[5,6]. Anwar and Hogarth[7] have studied dc electrical properties of MoO_3 films.

Vanadium pentoxide based transition metal oxide received particular attention to the study of electrical properties. Thin films of amorphous V_2O_5 exhibit semiconducting properties. This is due to the trapping of electrons between transition-metal ions in different valence states (V^{4+} and V^{5+}). The electron-phonon coupling being rather strong, the unpaired electrons trapped in their own polarisation wells and the charge carriers are actually small polarons[8]. The conductivity is then dominated by the thermally activated hopping of

these polarons. A localization of the charge carriers is observed in these amorphous films and their conductivity is about two orders of magnitude smaller than for crystalline V_2O_5[9,10]. Vanadium ions in different oxidation states yield semiconducting properties due to a hopping process of the unpaired 3d electron from a V^{4+} to a V^{5+} ion[11,12].

Orthorhombic V_2O_5 is the only stable phase at room temperature[13]. Several oxides of vanadium (VO, V_2O_3, VO_2, V_3O_5, V_6O_{13}, V_2O_5) undergo a transition from a metal to a semiconductor or insulator phase at critical temperatures. The change in crystal structure is accomplished by a large change in electrical behaviour. Therefore, these oxides have potential use, particularly, in thin film form, for a wide variety of applications involving thermally activated electronic or optical switching devices. DC conductivity of amorphous V_2O_5 film quickly decreases when the temperature decreases, and a non-linear plot of $\ln(\sigma T)$ vs T^{-1} is obtained. Such a behaviour is typical of amorphous transition metal oxides[8].

Morin[14] showed that the width of the 3d band decreases in the 3d oxide series from scandium to vanadium and it approaches zero for chromium oxide. Depending upon the width of the 3d band, conduction in these materials is attributed either to electrons in the 3d band of transition metal or to electron transitions between cations of different valencies. V_2O_5 is especially interesting in thin film form because of the possibility of integration into microelectronic circuitry. The generally accepted conductivity mechanism is that of trapping of electrons between transition metal ions in different valence states. Conductivity is due to the thermally activated migration of small polarons. At high temperature this results in a conductivity of the form given by the Arrhenius equation, but the observed activation energy is a temperature dependent.

Interaction between electron and optical phonons is strong in conduction through transition metal oxides. If the interaction is strong enough, small polarons will be formed and at sufficiently high

temperature this will move by hopping process. Bogomolov et al.[15,16] have discussed conduction in TiO_2 and given evidence for small polaron behaviour.

3.2. Experiment

Thin films of the MoO_3, V_2O_5, and TiO_2 are prepared using thermal evaporation described in section 2.4 (chapter II), in a vacuum of $2x10^{-5}$ mbar. Prior to the coating, either ends of the substrate is coated with high purity aluminium (Al) so as to get good ohmic contact. For MIM studies substrates previously coated with Al based electrode have been used. The evaporation is carried out using electron beam gun. Films are deposited onto glass substrates. The film thickness was noted by a quartz crystal thickness monitor and counter checked by multiple beam interferometry. The conductivity studies are carried out using the Keithley Electrometer. Capacitance variation of MIM with temperature and thickness of the film were studied. For each material the area of the insulator in the MIM structure was the same. Capacitance-voltage (C-V)

characteristic was studied by applying voltage across the capacitors.

3.3. Results and discussion.

3.3.1. DC electrical conductivity in coplanar geometry ($\sigma_{\parallel}$).

The DC conductivity is calculated from the current-voltage (I-V) measurements by knowing the area and thickness of the film. The temperature dependence of conductivity is given by Arrhenius relation given in equation 1.5 (section 1.8.3, Chapter I).

Figure 3.1 shows the temperature dependence of DC electrical conductivity (σ) of MoO_3 films for three different thicknesses 165, 187, and 208 nm respectively. The plot ln σ vs $10^3/T$ exhibits two straight line regions of different activation energies of conductivity for the same sample. The values of activation energy ΔE_1 in the lower temperature region (305-338 K) are 0.46, 0.43, and 0.41 eV for different thicknesses 165, 187, and 208 nm respectively. But the values of activation energy ΔE_2 in the higher temperature region

-3.5
-4
-5
-6
-7
-8

$\mathrm{Ln}\,\sigma\ (\Omega^{-1}m^{-1})$

● t = 165nm
+ t = 187nm
o t = 208nm

2.8 2.9 3.0 3.1 3.2 3.3

$10^3/T\ (K^{-1})$

Fig.3.1. Plot of log σ vs. 1/T for MoO_3 films of thicknesses 165nm, 187nm, and 208nm in coplanar geometry ($\sigma_{\parallel}$).

(338-348 K) are 1.35, 1.32, and 1.29 eV for films having thicknesses 165, 187, and 208 nm respectively. There is a slight change of activation energy with thickness of the film.

Figure 3.2 shows the temperature dependence of DC electrical conductivity of the V_2O_5 films for three different thicknesses 45, 74, and 164 nm respectively. The plot ln σ vs $10^3/T$ exhibits two straight line regions of different activation energies for the same samples. The values of activation energy ΔE_1 in the lower temperature range (300-350K) are 0.39, 0.31, and 0.27 eV for thicknesses 45, 74, and 164 nm respectively. The values of activation energy ΔE_2 in the higher temperature range (350-433 K) are 0.79, 0.52, and 0.29 eV for thicknesses 45, 74, and 164 nm respectively. This shows that at higher temperature range the activation energy changes considerably with thickness. It is seen that in the case of the sample with thickness 164 nm there is no considerable change between ΔE_1 and ΔE_2. For all samples activation energy decreases with increase in thickness.

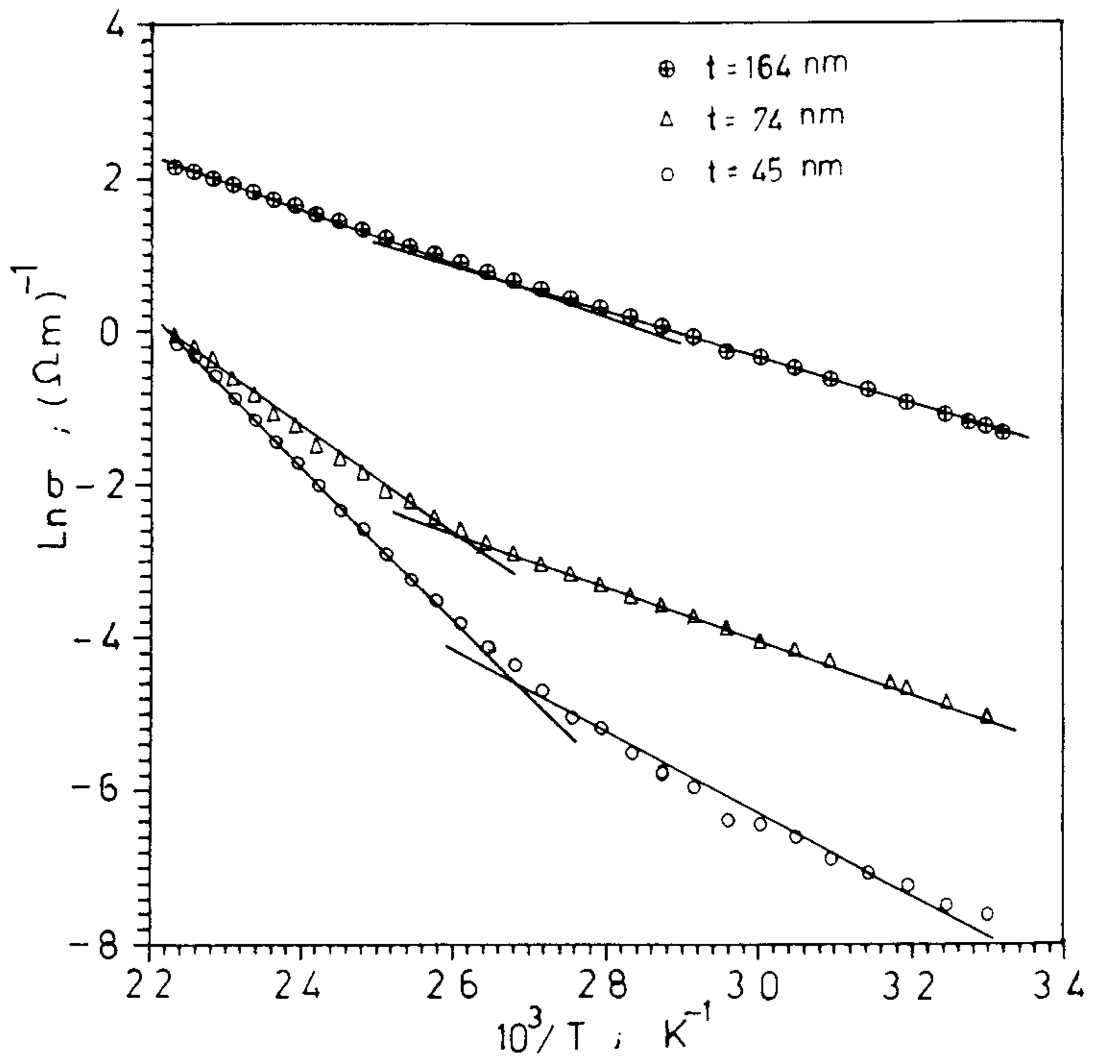

Fig.3.2. Plot of log σ vs. 1/T for V_2O_5 films of thicknesses 45nm, 74nm, and 164nm in coplanar geometry ($\sigma_{\parallel}$).

Figure 3.3 shows the temperature dependence of DC electrical conductivity of TiO_2 films for three different thicknesses 94, 110, and 153 nm respectively. The plot $\ln\sigma$ vs $10^3/T$ exhibits straight line for different thicknesses of TiO_2 samples. The values of activation energy ΔE in the temperature range (300-573 K) are 0.88, 0.86, and 0.83 eV for thicknesses 94, 110, and 153 nm respectively. This shows that activation energy decreases slightly with increase of thickness. The values of conductivity of TiO_2 films are in agreement with that reported by Nicoloso[17].

In all the cases activation energy is found to change with thickness of the film. In the case of MoO_3 the electrical transport depends upon the molybdenum present in the Mo^{5+} state and the transport mechanism involves the exchange of electrons between Mo^{5+} and Mo^{6+} ions. In the case of V_2O_5, the electrical transport depends upon the vanadium present in the V^{4+} state and the transport mechanism involves the exchange of electrons between V^{4+} and V^{5+} ions. In the case of a

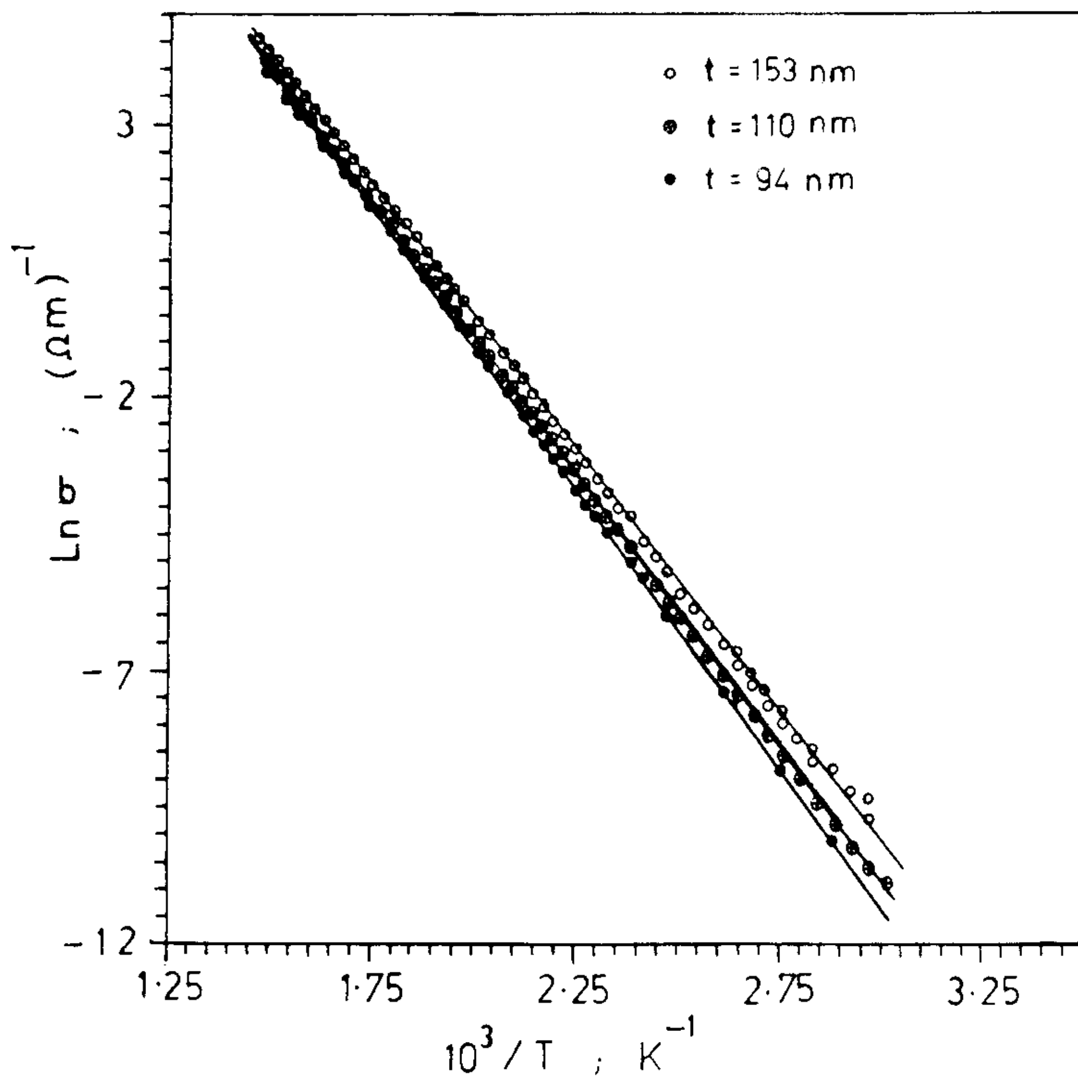

Fig.3.3. Plot of log σ vs. 1/T for TiO_2 films of thicknesses 94nm, 110nm and 153nm in coplanar geometry ($\sigma_{\parallel}$)

less thin film, less number of electrons get more quantity of heat energy. So there is a change of activation energy with thickness. In the case of V_2O_5 films a single molecule contains two vanadium atoms. So the number of electrons are large in V_2O_5. So activation energy of V_2O_5 is large in the higher temperature region.

In the case of TiO_2 single activation energy exists for each thickness. TiO phase may also be present in the TiO_2 film. These different valence states of TiO_2 produce excess electrons. In a less thin film less number of electrons get more heat energy. So the activation energy increases as the thickness decreases.

The decrease in activation energy with increase in film thickness is attributed to an increase in concentration of oxygen vacancies. The degree of localization of electrons increases with the increase of cation concentration, thereby increasing the number of donor centres. A large concentration of donor centres will effectively lower the activation energy.

Two types of localization processes[18] occur in amorphous transition metal oxides. The first type is the result of strong interaction of unpaired electron with the polar network leading to the formation of small polarons[8]. A polaron (an electron and its accompanying distortions) whose dimension is comparable to the lattice spacing is designated as a small polaron. The second type of localisation, known as `Anderson localisation' occurs due to the structural disorder[19]. The experimental data have been interpreted in terms of small polaron theory. A general formula was proposed by Mott[8,20] for the electrical conductivity in transition metal oxides.

$$\sigma = \frac{\nu_o N e^2 R^2 C (1-C)}{k T} \exp(-2 \alpha R) \exp(-\Delta E/k T) \quad \text{—— 3.1}$$

where ν_o is a phonon frequency, α the rate of wave-function decay, R the average hopping distance, ΔE thermal activation energy, N is the number of transition metal ion sites per unit volume, e is the charge, and k_B is the Boltzmann's constant. This equation is

comparable to Arrhenius equation 1.5 (section 1.8.3, chapter I). In the case of V_2O_5
$C = V^{4+}/(V^{4+}+V^{5+})$. Equation 3.1 can be written as

$$\ln(\sigma T) = \ln A - \Delta E/k_B T \qquad 3.2$$

Figure 3.4 is a plot of $\ln(\sigma T)$ vs $10^3/T$ for MoO_3 films of thicknesses 126, 150, 163 nm respectively. Straight line graph is obtained for each thickness of the sample. The values of activation energy obtained are 0.761, 0.750, 0.624 eV for thicknesses 126, 150, and 163 nm respectively.

Plot of $\ln(\sigma T)$ vs $10^3/T$ shown in figure 3.5 is for films of V_2O_5 of thicknesses 164, 254, and 299 nm respectively. The curves are linear, allowing to estimate thermal activation energy ΔE. The values of activation energy are 0.551, 0.327, and 0.233 eV for thicknesses 164, 254, and 299 nm respectively. Equation 3.1 is valid in the high temperature range[20] ($T > \theta_D$, where θ_D is the Debye temperature).

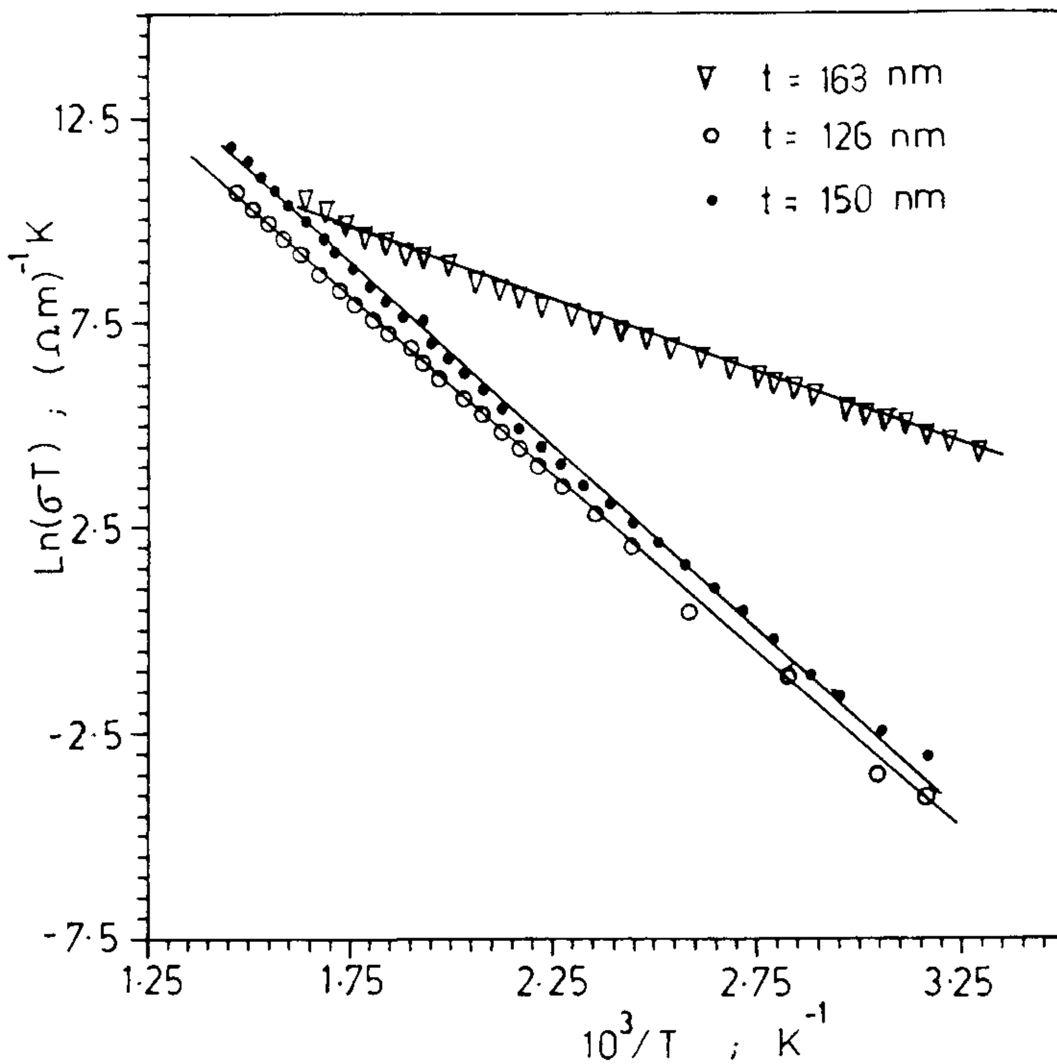

Fig.3.4. Plot of log(σ T) vs. 1/T for MoO_3 films of thicknesses 126nm, 150nm, and 163nm according to Mott's formula.

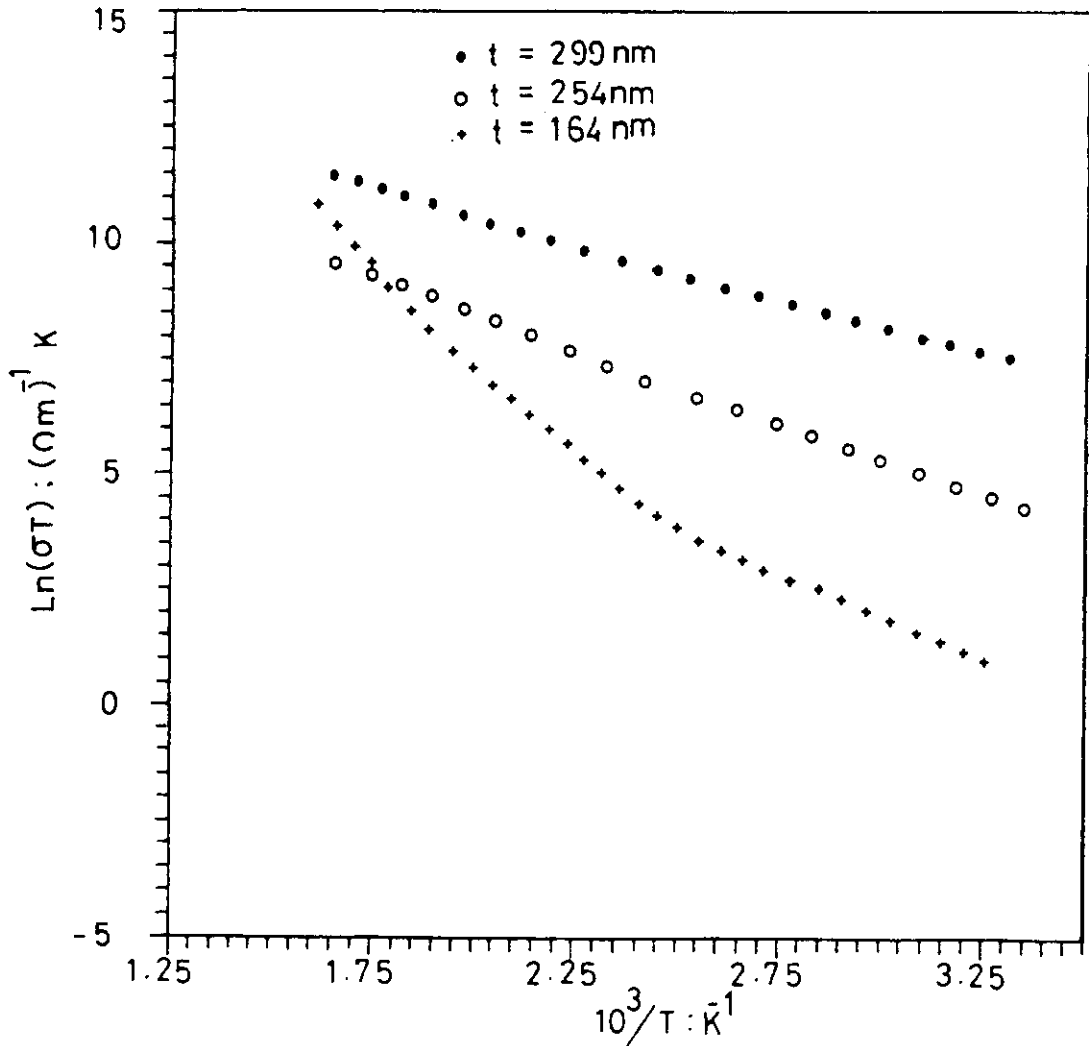

Fig.3.5. Plot of log (σ T) vs. 1/T for V_2O_5 films of thicknesses 164nm, 254nm, and 299nm according to Mott's formula.

Plot of $\ln(\sigma T)$ vs $10^3/T$ shown in figure 3.6 is for TiO_2 films of thicknesses 94, 110, and 153 nm respectively. The values of the activation energy obtained are 0.929, 0.899, and 0.874 eV for thicknesses 94, 110, and 153 nm respectively.

The thermal activation energy $\Delta E = \Delta E_h + (1/2) \Delta E_d$,where ΔE_h corresponds to the small polaron formation in the absence of any disorder while ΔE_d corresponds to the random disorder[21]. Actually ΔE_d is the minimum energy necessary for coupling to adjacent wells of the same depth.

3.3.2. DC electrical conductivity in sandwich geometry ($\sigma_\perp$)

The DC electrical conductivity is measured for MIM structure of the films of known area and thickness. Here the electrical conductivity is measured in the perpendicular direction and hence it is noted as $\sigma_\perp$ for Al-MoO_3-Al, Al-V_2O_5-Al, and Al-TiO_2-Al samples. Electrical conductivity is measured in V/I mode using Kiethly elctrometer applying a voltage of 0.75V in

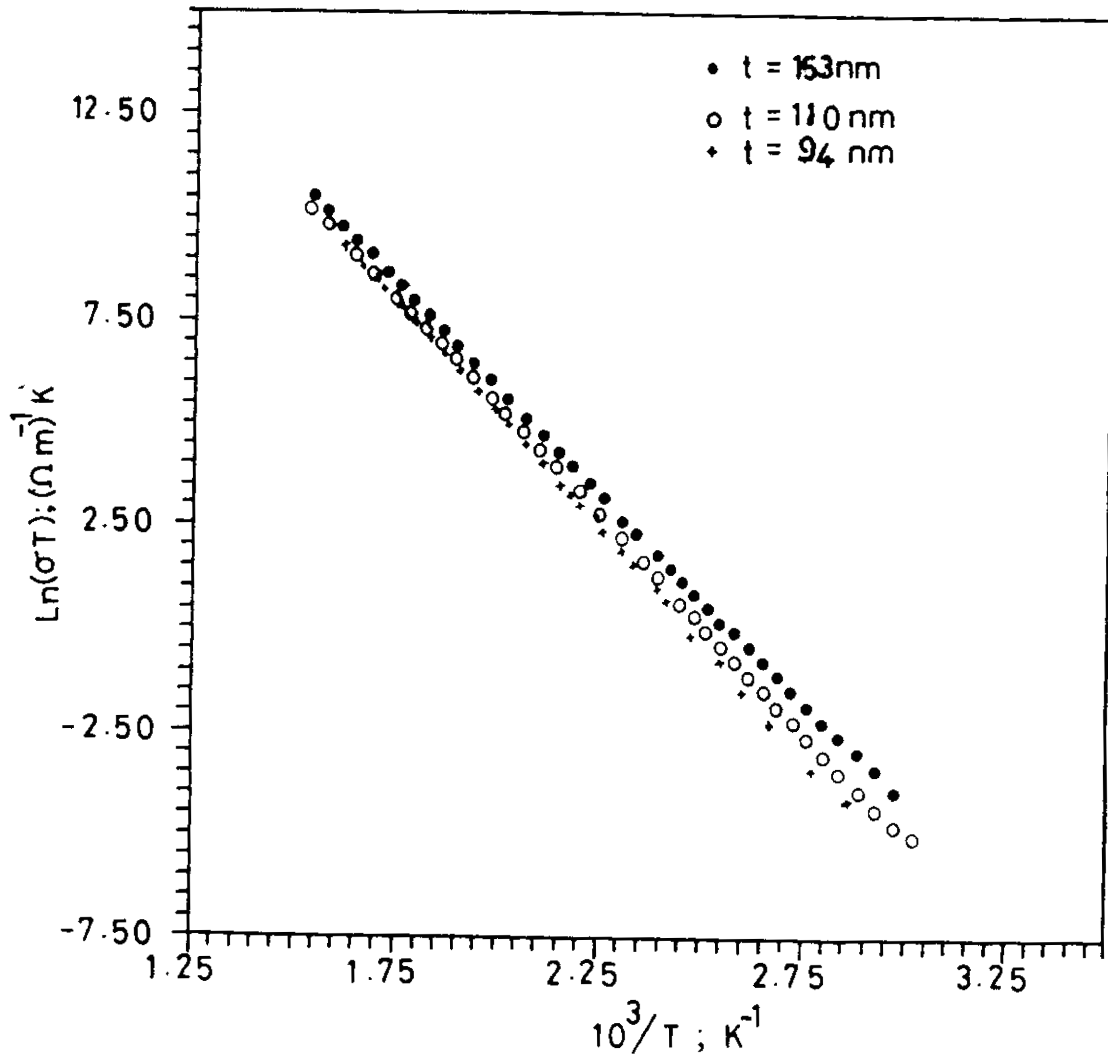

Fig.3.6. Plot of log (σ T) vs. 1/T for conductivity of TiO_2 films of thicknesses 94nm, 110nm, and 153nm according to Mott's formula.

between the metal electrodes.

Figure 3.7 is the plot of ln σ vs $10^3/T$ for the films of MoO_3 of thicknesses 131, 156, and 194 nm respectively in the MIM sandwich form. Here the curves obtained are **found** to be linear. The values of activation energies are 0.736, 0.472, and 0.164 eV for thicknesses 131, 156, and 194 nm respectively. Here the activation energy decreases with increase of film thickness. On comparison of conductivity of the sandwich geometry $\sigma_\perp$ to the conductivity in coplanar geometry $\sigma_\parallel$ from figure 3.1, it is observed that $\sigma_\perp$ is much lower than σ for the same temperature.

Figure 3.8 shows the plot of temperature dependence of DC electrical conductivity of V_2O_5 films in sandwich geometry for three different thicknesses 127, 143, and 164 nm respectively. The curves can be connected by a best fit line. The values of activation energy are 0.282, 0.269, and 0.132 for thicknesses 127, 143, and 164 nm respectively. Comparing the conductivity in the sandwich geometry $\sigma_\perp$ to the conductivity $\sigma_\parallel$ from figure 3.2, it is observed that $\sigma_\perp$

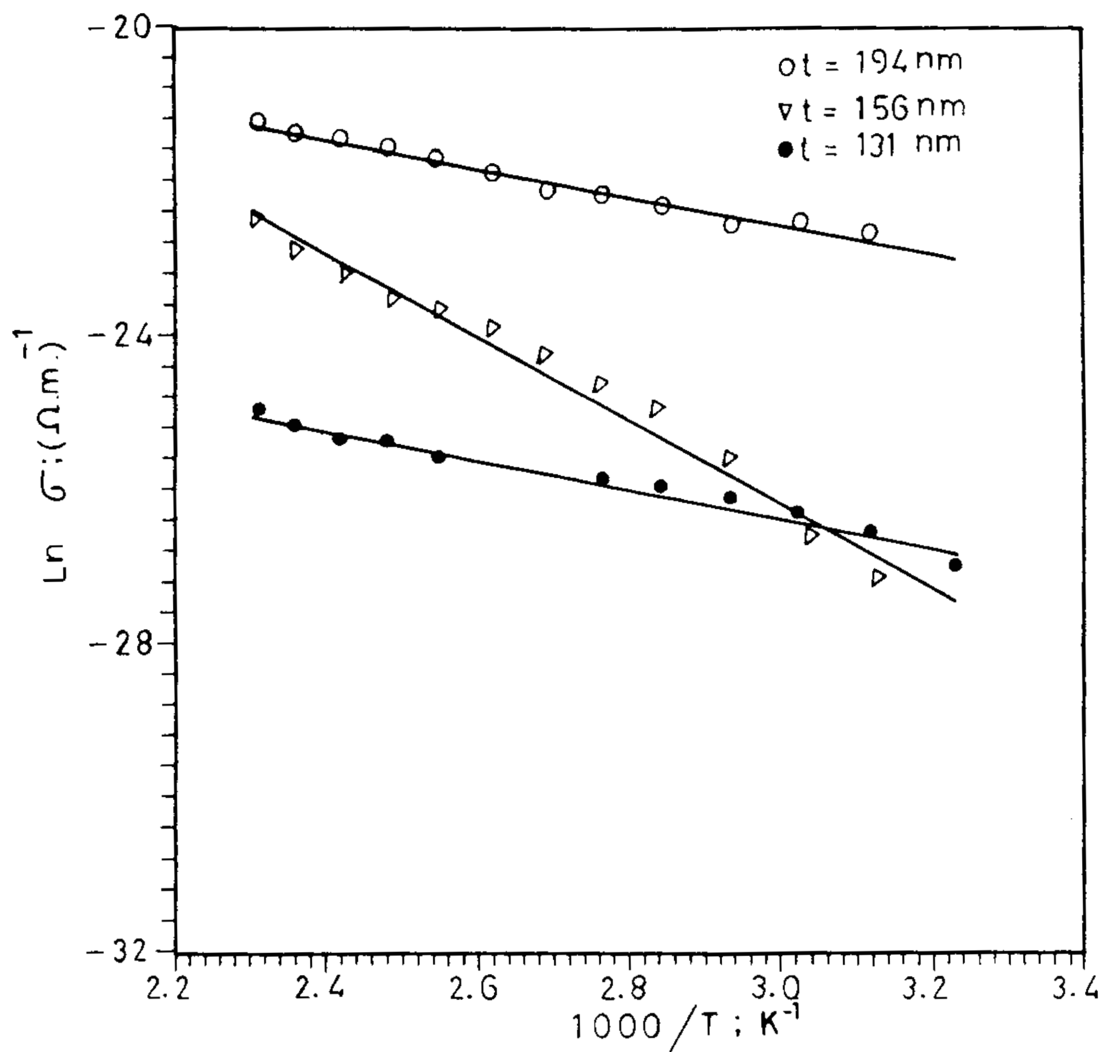

Fig.3.7. Plot of log σ vs. 1/T for MoO_3 film of thicknesses 131nm, 156nm, and 194nm in sandwich geometry ($\sigma_{\perp}$).

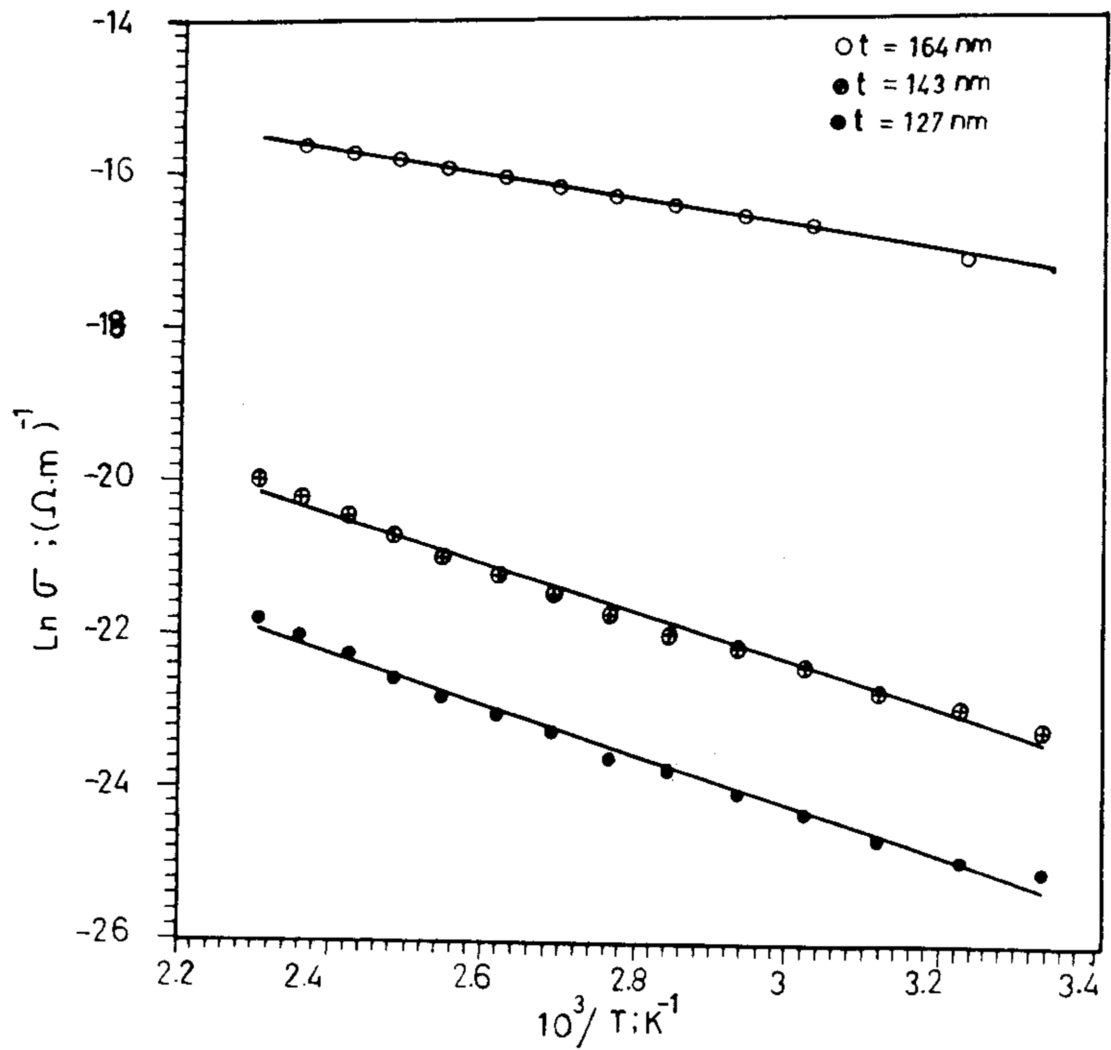

Fig.3.8. Plot of log σ vs. 1/T for V_2O_5 films of thicknesses 127nm, 143nm, and 164 nm in sandwich geometry (σ_1)

is much lower than $\sigma_{\parallel}$ for the same temperature.

Figure 3.9 shows the plot of temperature dependence of DC electrical conductivity of TiO_2 films in sandwich geometry for three different thicknesses 60, 110, and 153 nm respectively. Activation energy can be calculated by connecting the curves using best fit lines. The values of activation energy obtained are 0.282, 0.184, and 0.194 eV for thicknesses 60, 110, and 153 nm respectively. Comparing the conductivity in the sandwich geometry $\sigma_{\perp}$ to the conductivity in coplanar geometry $\sigma_{\parallel}$ from figure 3.3, it is observed that $\sigma_{\perp}$ is much lower than $\sigma_{\parallel}$ for the same temperature.

Figure 3.10 is the modified plot of figure 3.7 using $\ln(\sigma T)$ vs $10^3/T$ for MoO_3 films. The values of activation energy are 0.175, 0.478, and 0.168 eV for thicknesses 131, 156, and 194 nm respectively.

Figure 3.11 is the modified plot of figure 3.8 using $\ln(\sigma T)$ vs $10^3/T$ for V_2O_5 films. The curves are much more linear than that at figure 3.8. The values of activation energy are 0.312, 0.300, and 0.163 eV for thicknesses 127, 143, and 164 nm respectively.

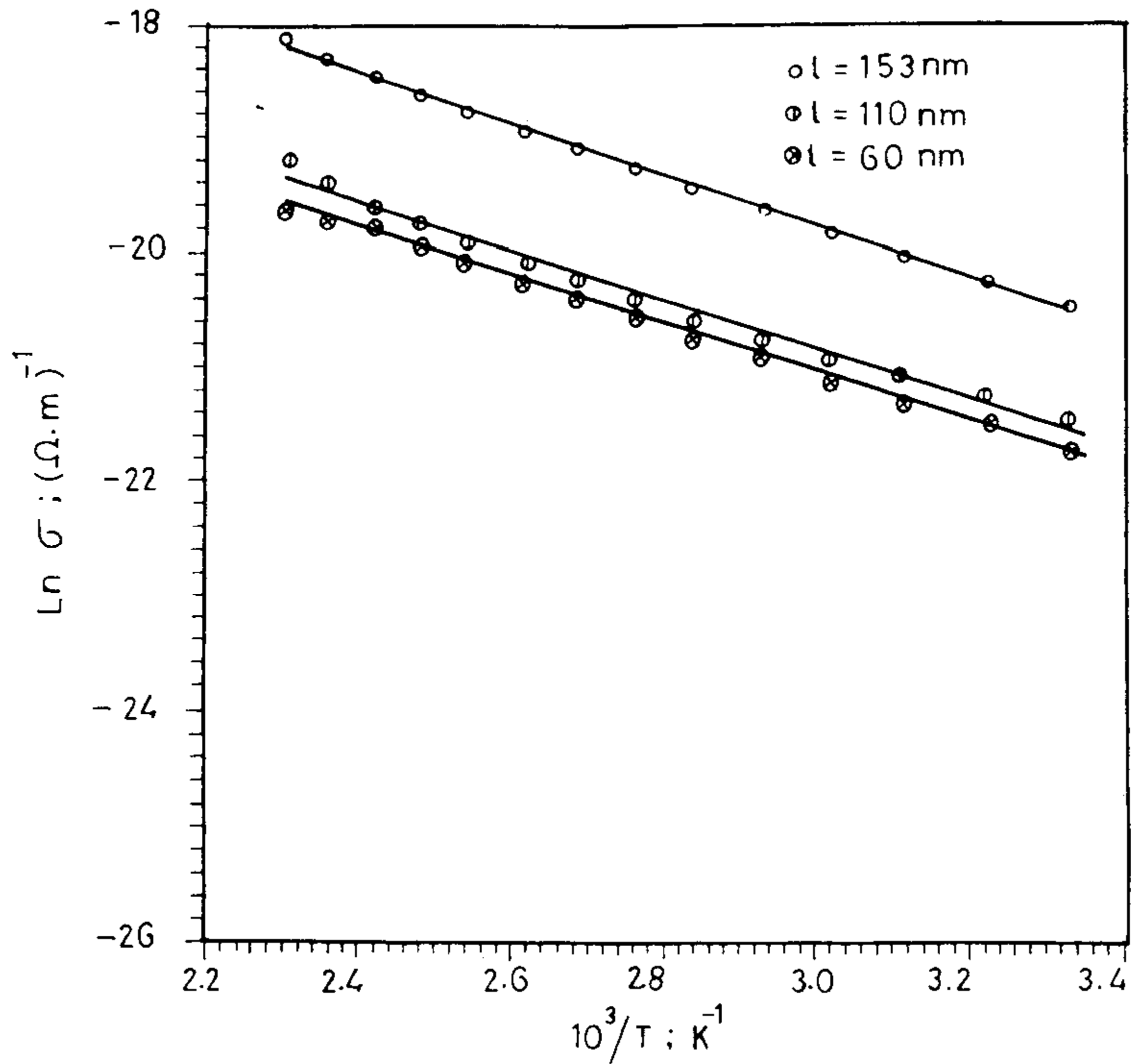

Fig.3.9. Plot of log σ vs. 1/T for TiO_2 film of thicknesses 60nm, 110nm and 153nm in sandwich geometry ($\sigma_\perp$).

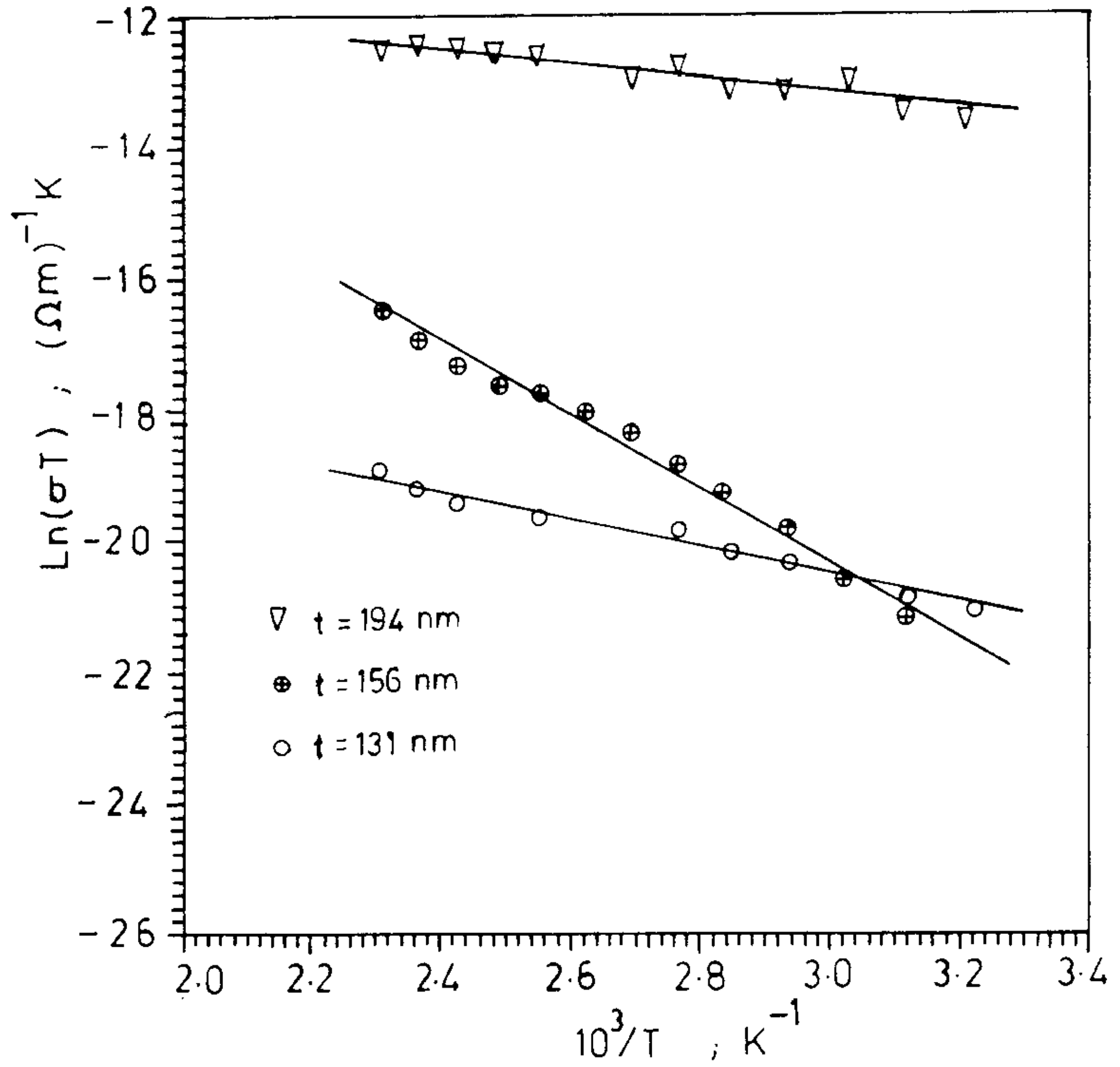

Fig.3.10. Plot of log (σ T) vs. 1/T for MoO_3 films of thicknesses 131nm 156nm, 194nm in sandwich geometry according to Mott's formula.

Fig.3.11. Plot of log (σ T) vs. 1/T for V_2O_5 films of thicknesses 127nm, 143nm, and 164 nm in sandwich geometry according to Mott's formula.

Figure 3.12 is the modified plot of figure 3.9 using $\ln(\sigma T)$ vs $10^3/T$ for TiO_2. The values of activation energy are 0.213, 0.215, and 0.225 eV for thickness 60, 110, and 153 nm respectively.

It is observed that conductivity is much lower when it is measured in sandwich geometry than in the coplanar geometry which is in agreement with the results obtained by Bullot et al.[22] for V_2O_5 films. This shows that conductivity has anisotropy in the thin film state. This may be due to the fact that the disorder in the field direction is larger in $\sigma_{\perp}$ than in $\sigma_{\parallel}$. This can also be correlated with structure: in the coplanar geometry conductivity is dominated by polaron hopping along the fibers which are well organised[23]. In contrast in the sandwich geometry hopping between different layers is needed.

3.3.3. Field dependent electrical conduction in Metal-Insulator-Metal structure.

Room temperature current-voltage characteristics of Al-MoO_3-Al are shown in figure 3.13 for three different MoO_3 thicknesses 156, 181, and 194 nm

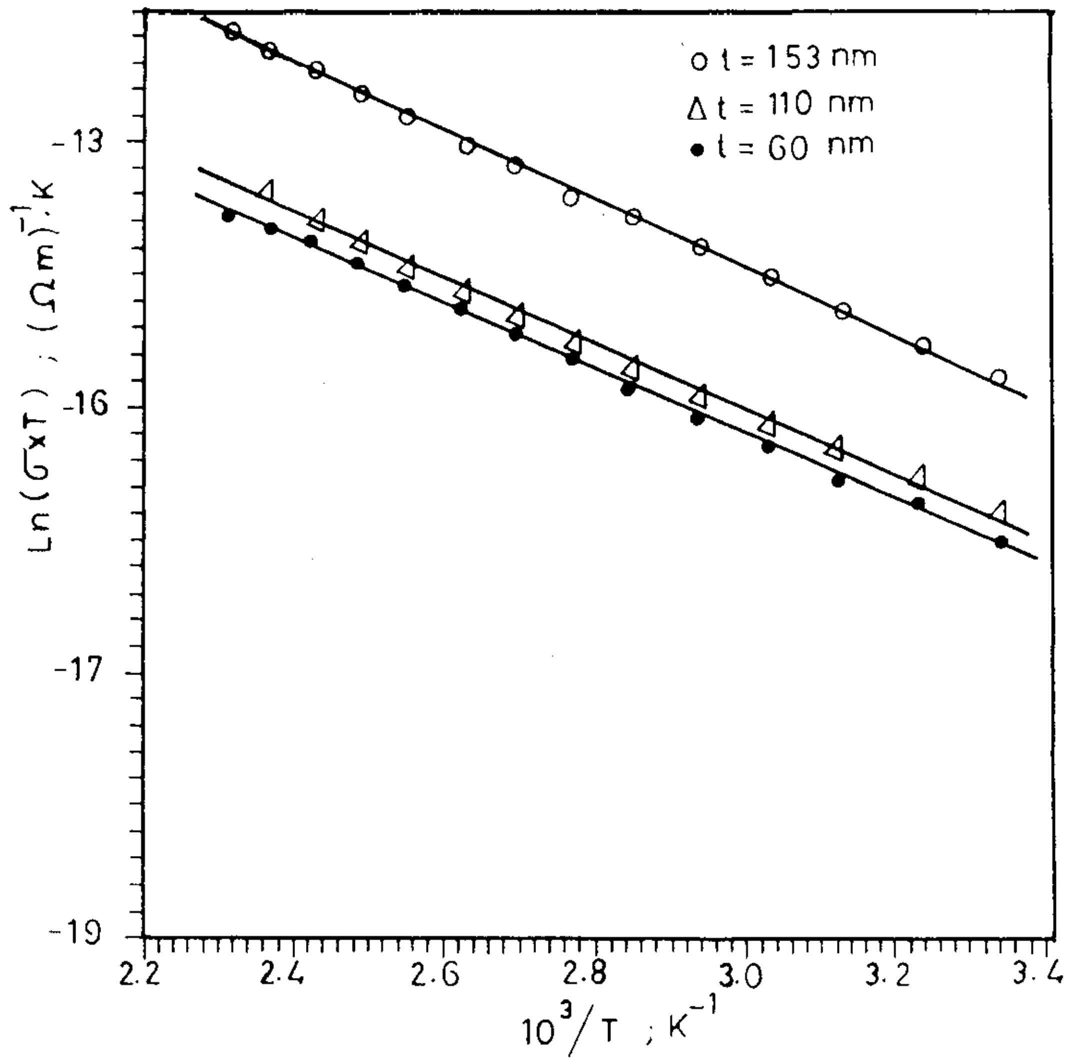

Fig.3.12. Plot of log (σ T) vs. 1/T for TiO_2 films of thicknesses 60nm, 110nm, and 153nm in sandwich geometry according to Mott's formula.

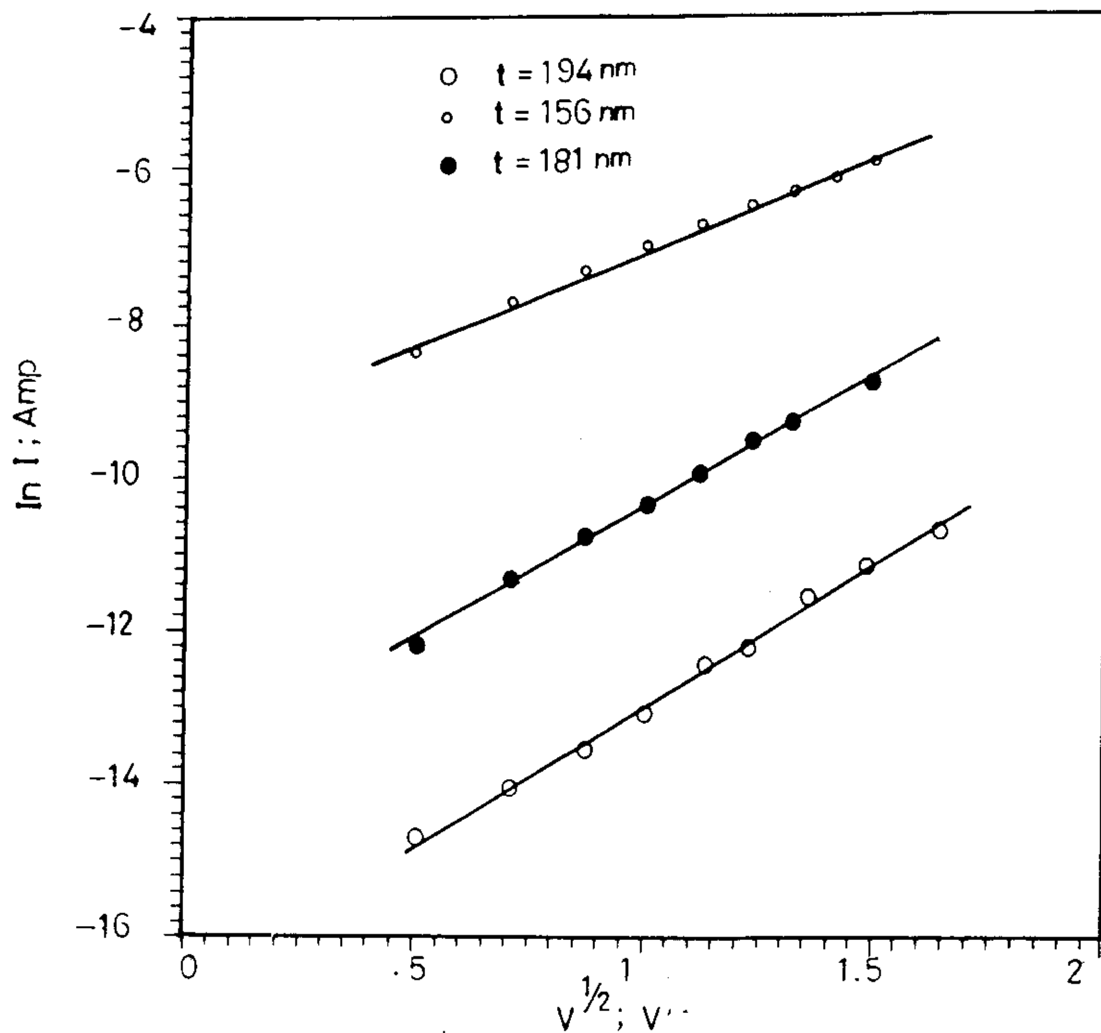

Fig.3.13. Plot of log I vs. $V^{1/2}$ for Al-MoO_3-Al films of thicknesses 156nm, 181nm, and 194nm at room temperature.

respectively as lnI vs $V^{1/2}$. The plots are found to be linear.

Current-voltage characteristics of Al-V_2O_5-Al at room temperature are shown in figure 3.14 for three different V_2O_5 thicknesses 113, 127, and 162 nm respectively as ln I vs $V^{1/2}$. The resulting curves are straight lines.

Figure 3.15 gives the current-voltage characteristics of Al-TiO_2-Al at room temperature for three different TiO_2 thicknesses 60, 110, and 153 nm respectively as lnI vs $V^{1/2}$. The resulting graphs show linearity.

In all the cases the graphs obtained are straight lines. The straight line behaviour of the curves may be explained by Poole-Frenkel bulk mechanism or Schottky emission at the electrode. In the Poole-Frenkel mechanism, the conduction is limited by the field-enhanced thermal emission of the electrons from the discrete trap level into the conduction band. In the Schottky emission process, the electrons are emitted from the metal electrode into the conduction

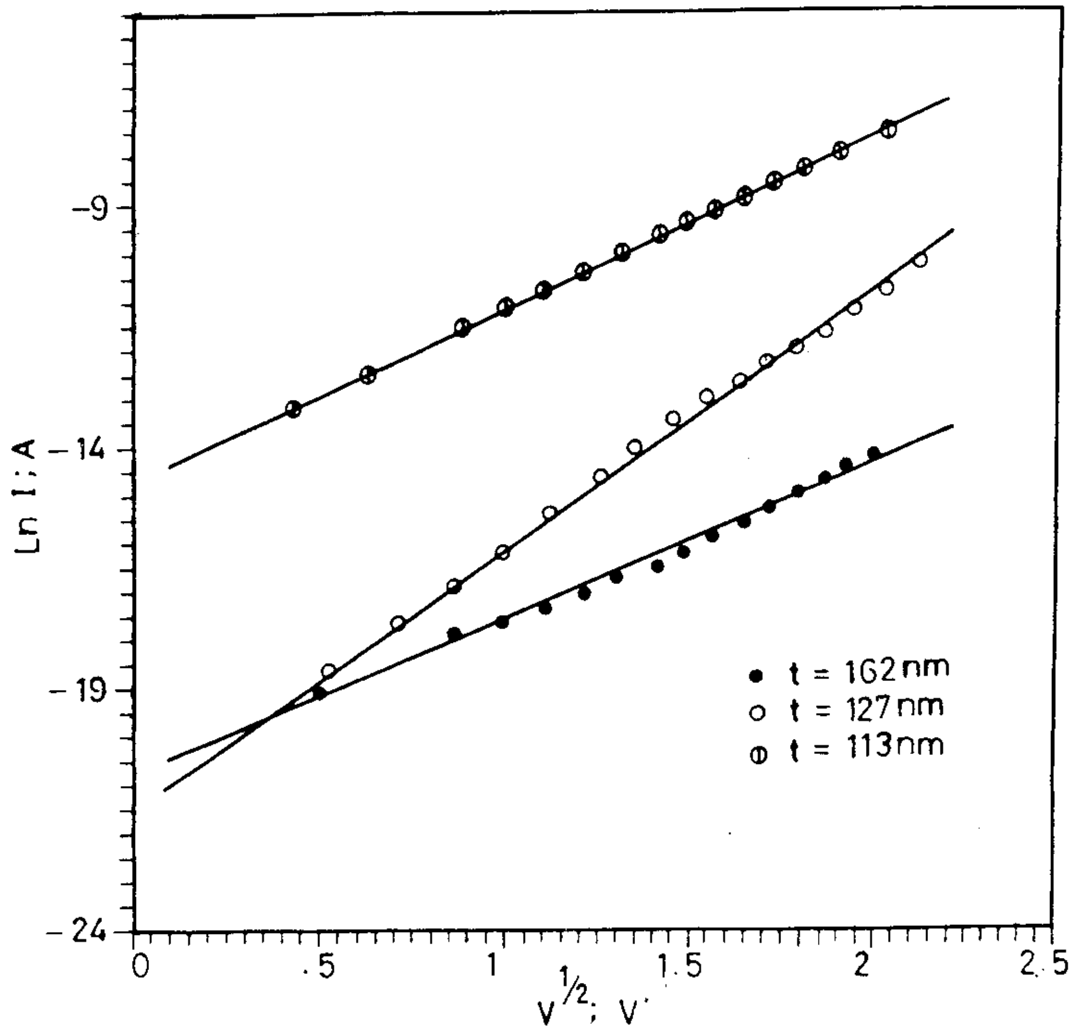

Fig.3.14. Plot of ln I vs. $V^{1/2}$ for Al-V_2O_5-Al films of V_2O_5 thicknesses 113nm, 127nm, and 162nm at room temperature.

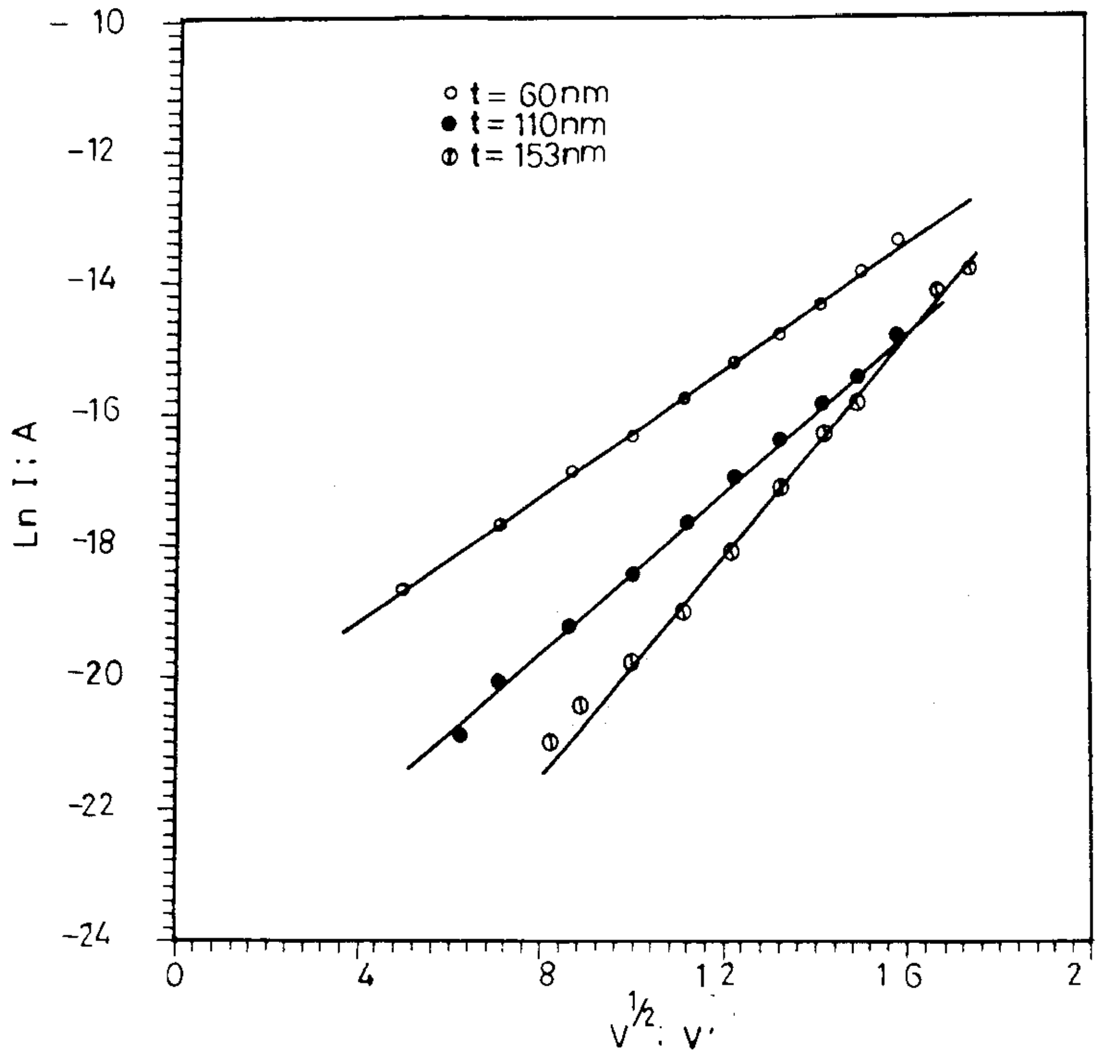

Fig.3.15. Plot of log I vs. $V^{1/2}$ for Al-TiO_2-Al films of TiO_2 thicknesses = 60nm, 110nm, and 153 nm at room temperature.

band of the insulating film over the image force interfacial barrier under attendant lowering of the applied electric field[24].

Many workers[25-28] have shown that current-voltage relationship of dielectric and semiconducting thin films is of the form[26-29]

$$I = A T^2 \exp\left[(\beta_s V^{1/2} - \phi_o) / k_B T \right] \quad \text{—— -3.3}$$

(Schottky emission)

$$I = B \exp\left[(\beta_{PF} V^{1/2} - \phi_i) / k_B T \right] \quad \text{———— 3.4}$$

(Poole-Frenkel emission)

$$\text{where} \quad \beta_{PF} = 2\beta_s = 2\left[\frac{e^3}{4\pi \varepsilon \varepsilon_o t} \right]^{1/2}$$

and e is the electronic charge, t is the thickness of the film, k_B is the Boltzmann's constant, ε_o is the dielectric constant and ε is the relative dielectric constant of the film. β_s is the Schottky barrier-

lowering coefficient at the metal-insulator interface and β_{PF} is the Poole-Frenkel barrier-lowering coefficient of the donor centres. ϕ_0 is the interfacial barrier height and ϕ_1 is the energy difference between the trap level and the bottom of the conduction band.

For fulfilment of the Schottky emission, the extrapolation of the linear plots for a common barrier and various thickness should pass through a single voltage at V = 0. This is not observed in the cases of MoO_3, V_2O_5, and TiO_2 films. Figure 3.16 gives the plot of ln (I/T^2) vs $10^3/T$ for Al-MoO_3-Al sample of MoO_3 thickness 156 nm for different biasing voltages varied from 0.25 to 1.5 V. The plot ln(I/T^2) vs $10^3/T$ shown in figure 3.17 is for Al-V_2O_5-Al sample of V_2O_5 thickness 162 nm for different biasing voltages varied from 0.25 to 1.5V. The plot of ln(I/T^2) vs $10^3/T$ for different biasing voltages varied from 0.25 to 1.5V shown in figure 3.18 is for Al-TiO_2-Al sample of TiO_2 thickness 153 nm. The basic requirement of Schottky emission is that the plot ln (I/T^2) vs $10^3/T$ should be straight line at fixed bias voltage as per equation 3.3. In the cases

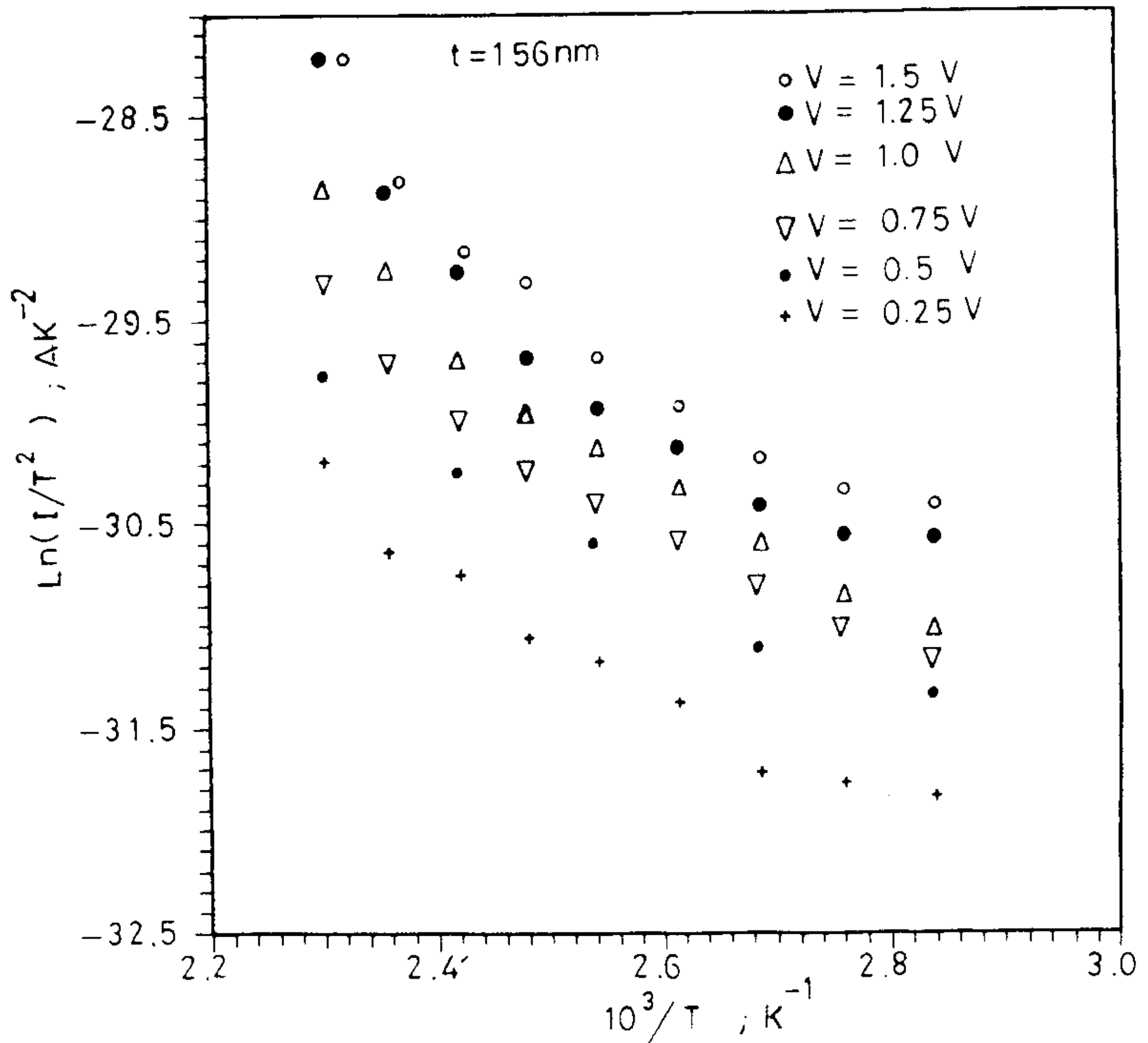

Fig.3.16. plot of ln (I/T^2) vs. $10^3/T$ at different biasing voltages for Al- MoO_3-Al film of MoO_3 thickness 156nm.

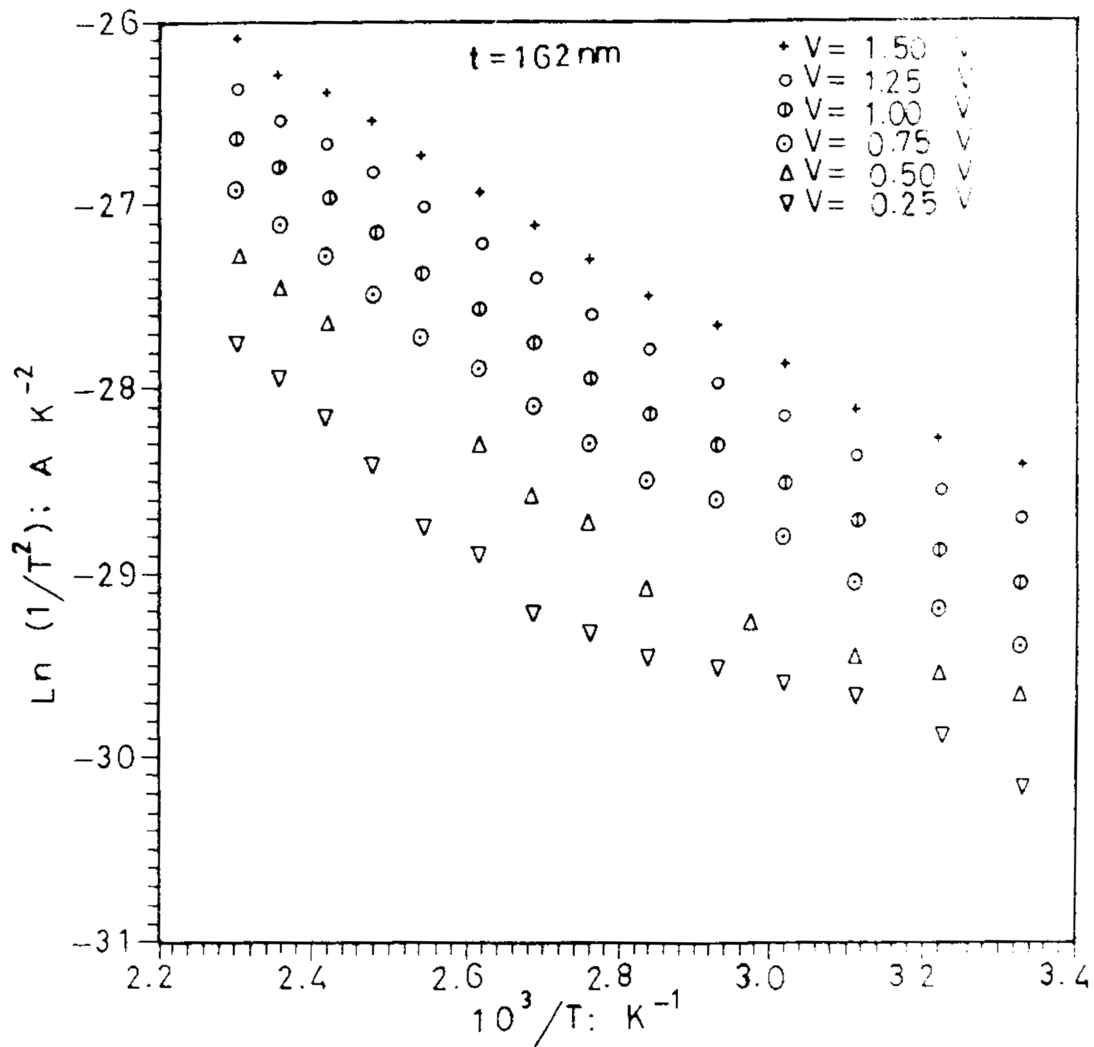

Fig.3.17. Plot of ln (I/T^2) vs. $10^3/T$ at different biasing voltages for Al-V_2O_5-Al film with V_2O_5 thickness 162nm.

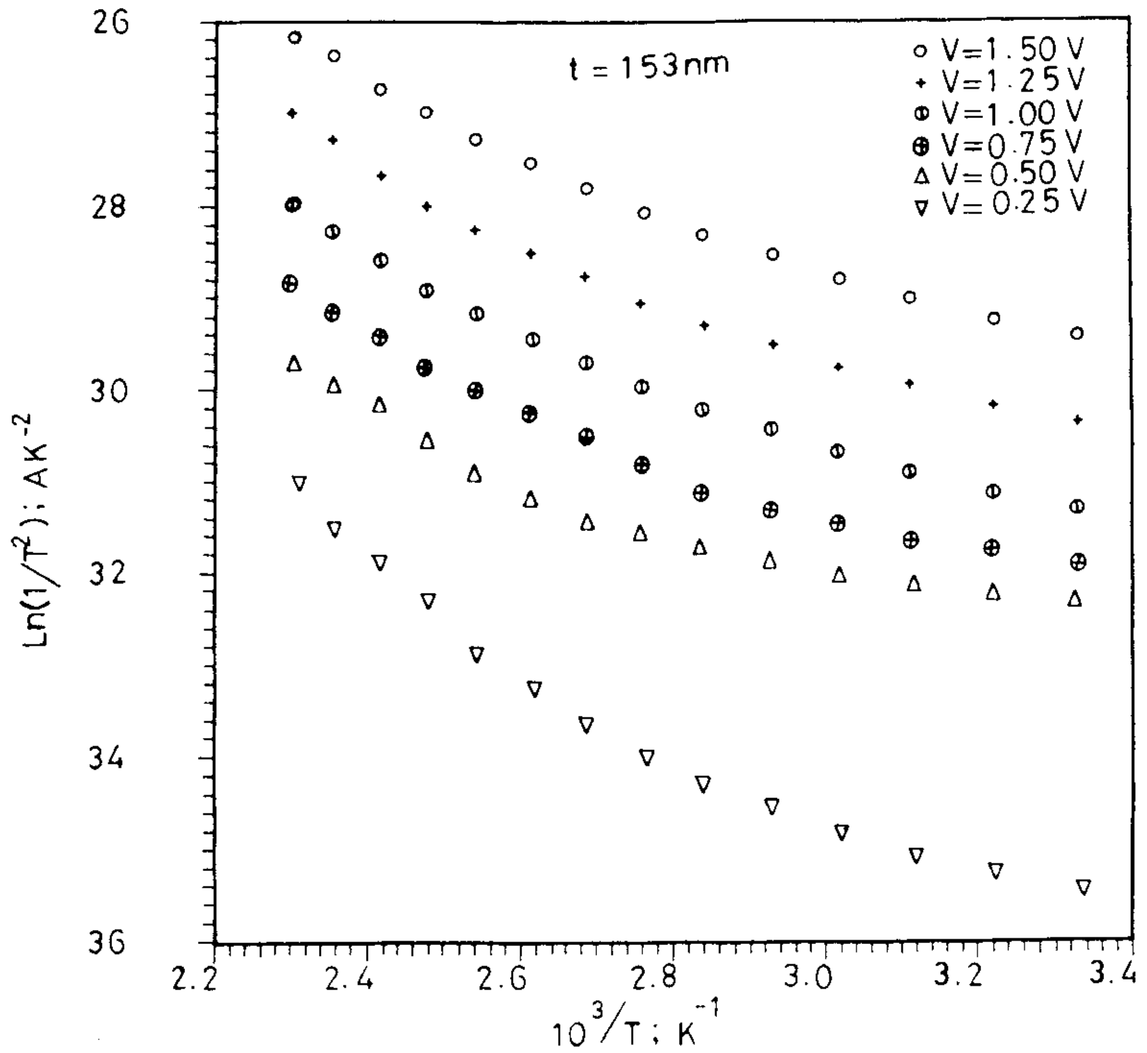

Fig.3.18. Plot of ln (I/T^2) vs. $10^3/T$ at different biasing voltages for Al-TiO_2-Al film with TiO_2 thickness 153nm.

T245

of MoO_3 and TiO_2 films the plots are in straight lines. So the conduction mechanism in MoO_3 and TiO_2 films are Poole-Frenkel type. But in the case of V_2O_5 film the points are found to be in a straight line at high field. So it is concluded that in the case of V_2O_5 films at high field the conduction mechanism is Poole-Frenkel type and at low field it is Schottky type.

Figure 3.19 shows a plot of ln I vs $10^3/T$ for Al-MoO_3-Al sample of MoO_3 thickness = 156 nm for different biasing voltages varied from 0.25 to 1.5V. The plot of ln I vs $10^3/T$ shown in figure 3.20 is for Al-V_2O_5-Al sample with V_2O_5 thickness = 162 nm for different biasing voltages, varied from 0.25 to 1.5V. Figure 3.21 gives the plot of Al-TiO_2-Al sample of TiO_2 thickness = 153 nm for different biasing voltages varied from 0.25 to 1.5V. The slope of the straight line has been measured and the thermal activation energy ΔE is calculated. It is found that the activation energy has two values as ΔE_1 for lower temperature region and ΔE_2 for higher temperature region. So it is concluded that activation energy depends slightly on applied field.

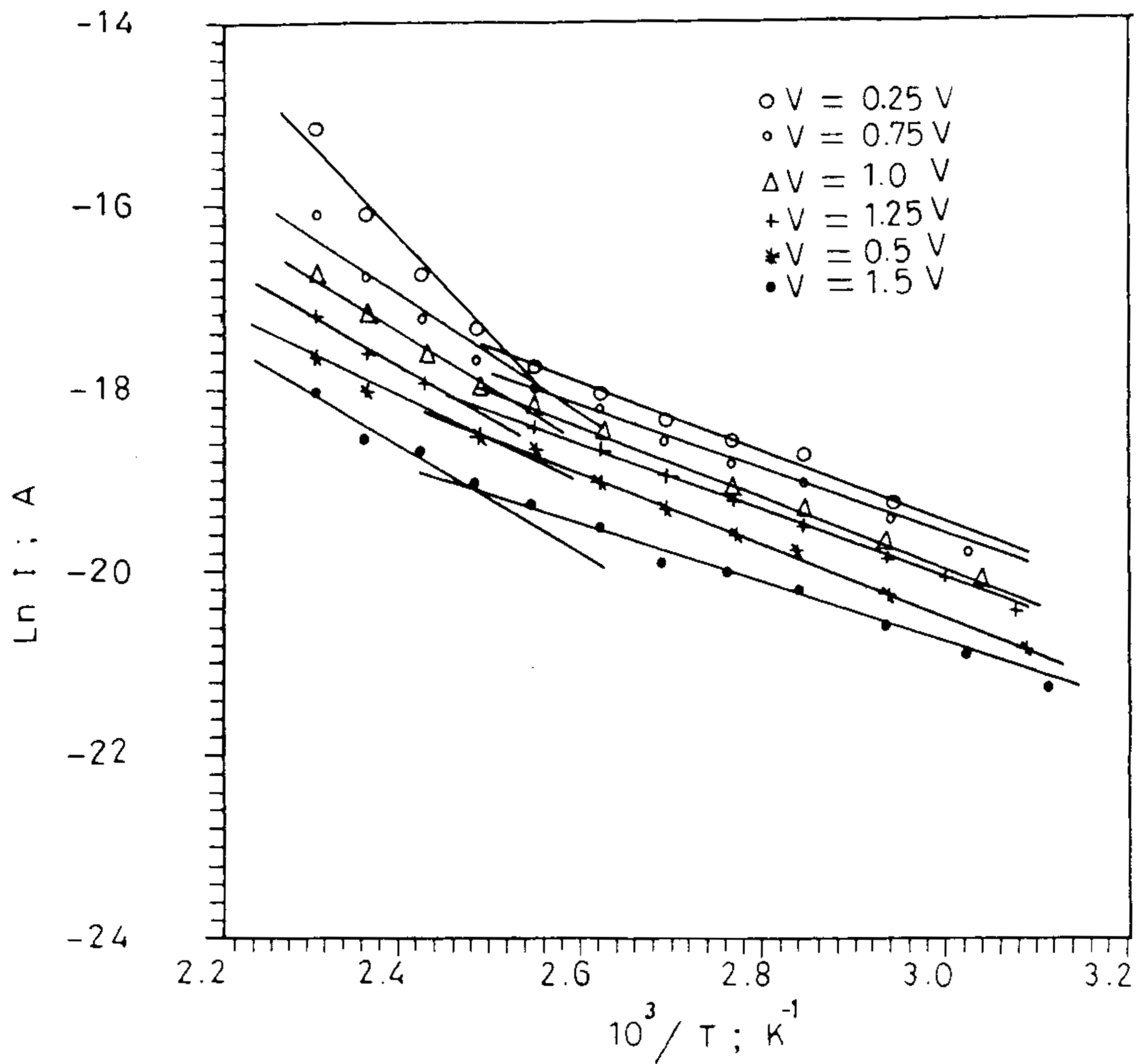

Fig.3.19. Plot of ln I with 10^3/T at different biasing voltages for Al-MoO_3-Al film with MoO_3 thickness 156nm.

Al-MoO_3-Al

Fig.3.19a. Plot of activation energy vs. biasing voltages for Al-MoO_3-Al sandwich structure with MoO_3 thickness = 156nm

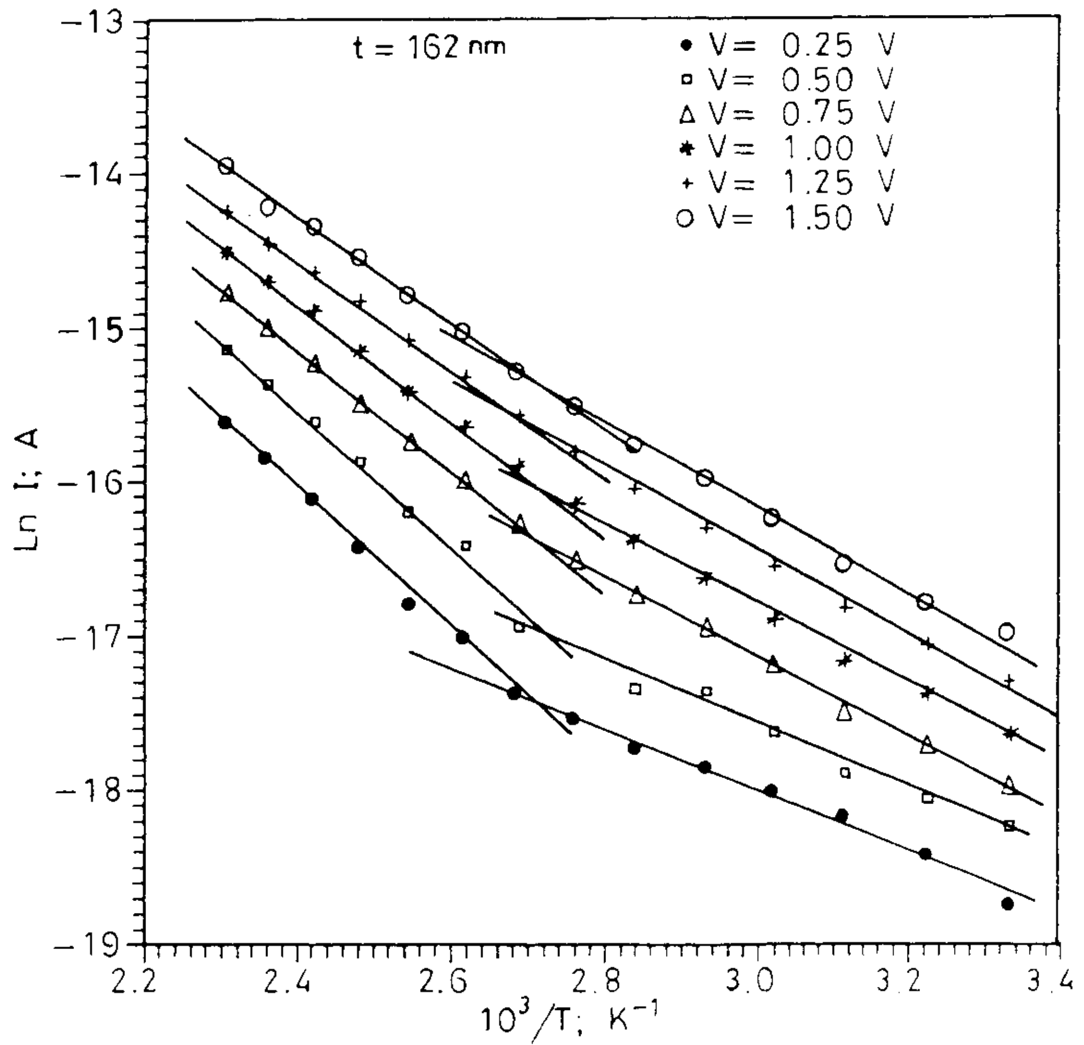

Fig.3.20. Plot of ln I with $10^3/T$ at different biasing voltages for Al-V_2O_5-Al film with V_2O_5 thickness 162nm.

25 Years

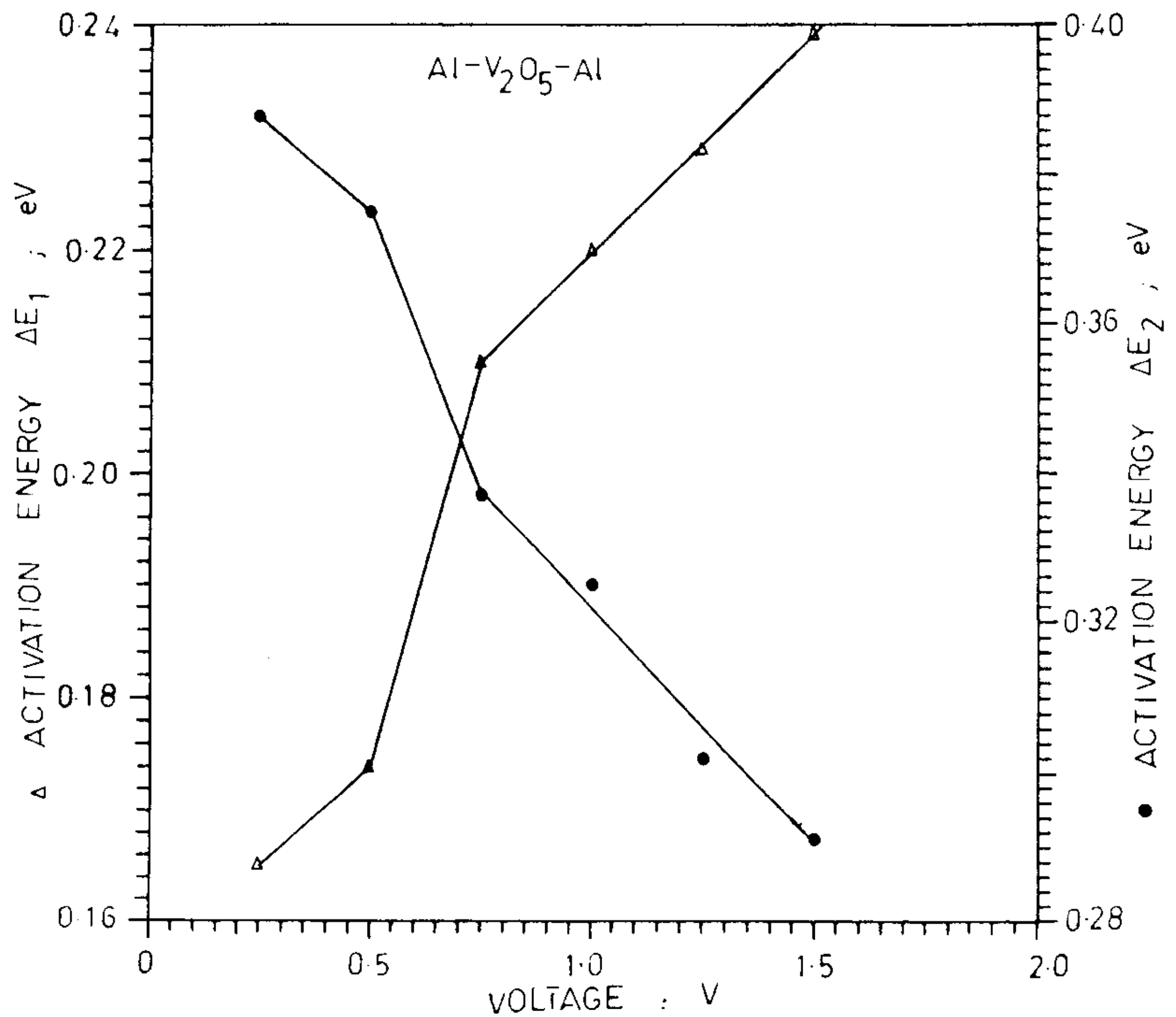

Fig.3.20a. Plot of activation energy vs. biasing voltages for Al-V_2O_5-Al sandwich structure with V_2O_5 thickness = 162nm.

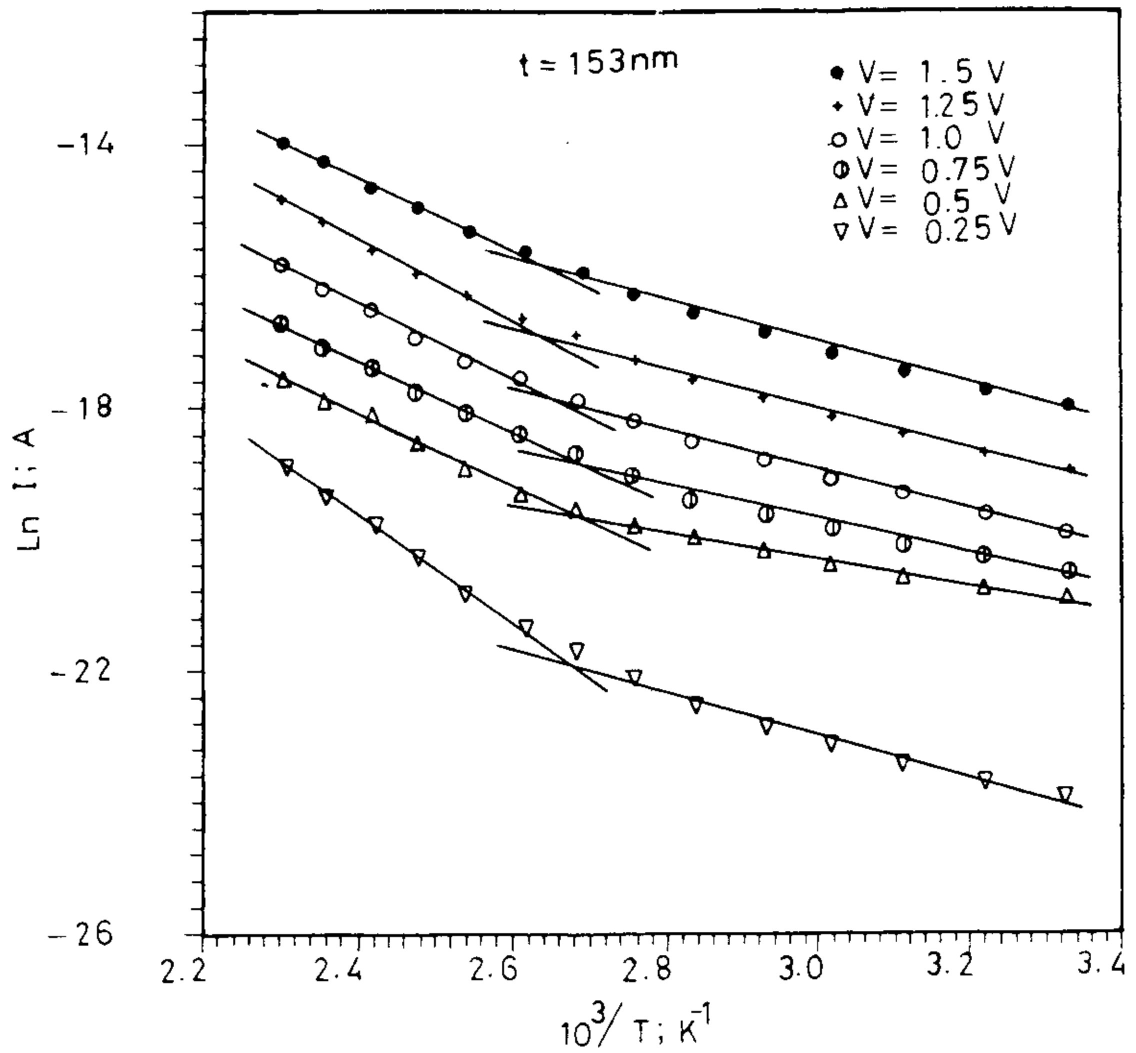

Fig.3.21. Plot of ln I vs. $10^3/T$ at different biasing voltages for Al-TiO_2-Al film with TiO_2 thickness 153nm.

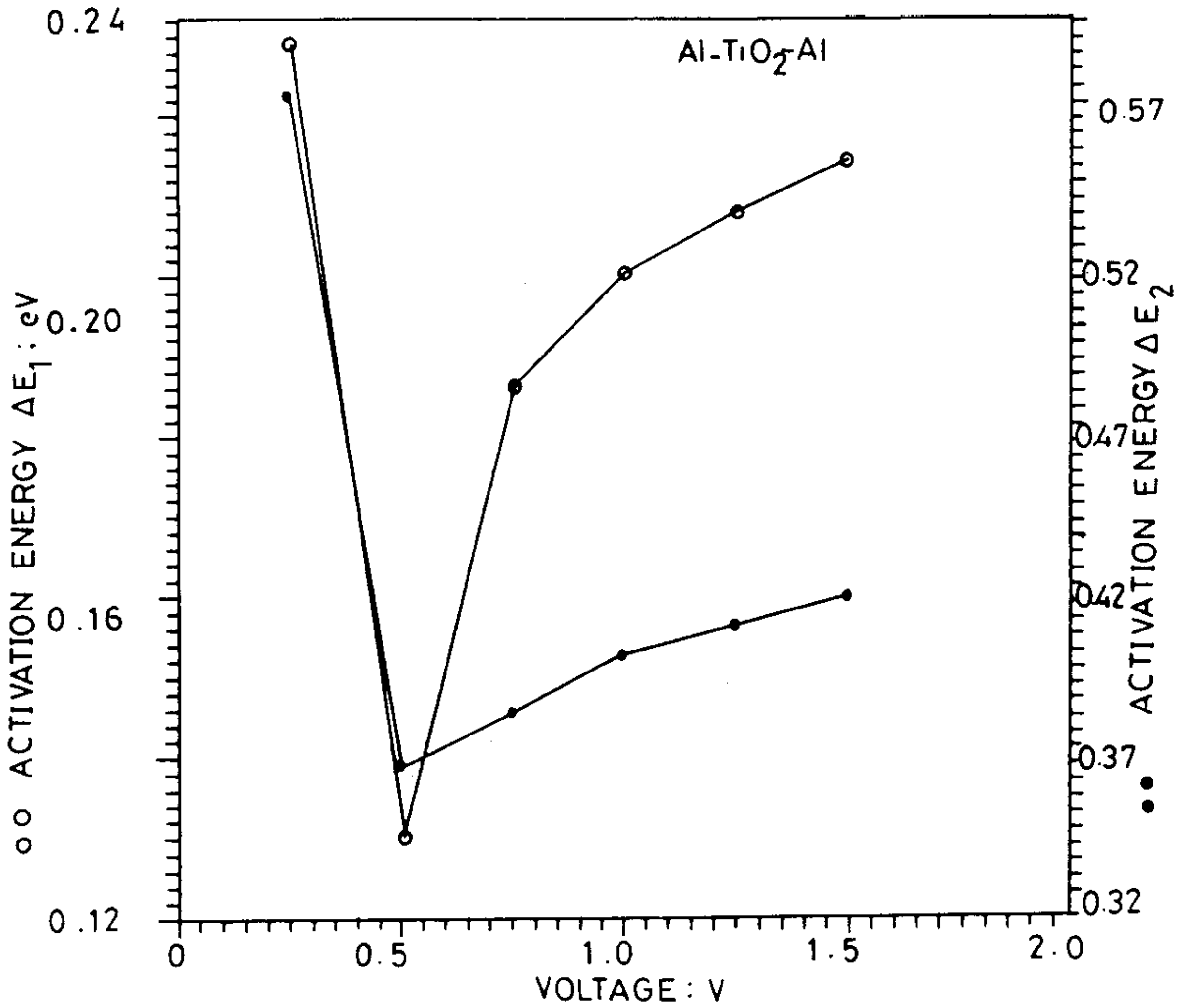

Fig.3.21a. Plot of activation energy vs. biasing voltages for Al-TiO_2-Al sandwich structure of TiO_2 thickness = 153nm

Figure 3.19a gives the variation of activation energy of MoO_3 sandwich structure with biasing voltage. The variation of activation energy of V_2O_5 with biasing voltage is shown in figure 3.20a and the variation of activation energy with biasing voltages for TiO_2 sandwich structure is given in figure 3.21a.

3.3.4. Studies of capacitance in Metal-Insulator-Metal structure.

Figure 3.22 shows the variation of capacitance with temperature of Al-MoO_3-Al where MoO_3 has thickness 131, 156, and 194 nm. From temperature 360K onwards the capacitance increases and becomes much faster from 400K onwards. In the case of film thickness = 194 nm the variation is little.

The variation of capacitance with temperature of Al-V_2O_5-Al where V_2O_5 has thicknesses 81, 113, and 164 nm is shown in figure 3.23. The variation of capacitance with temperature becomes faster from temperature 380K ownwards. Lesser the thickness of V_2O_5 film the greater is the variation of capacitance with

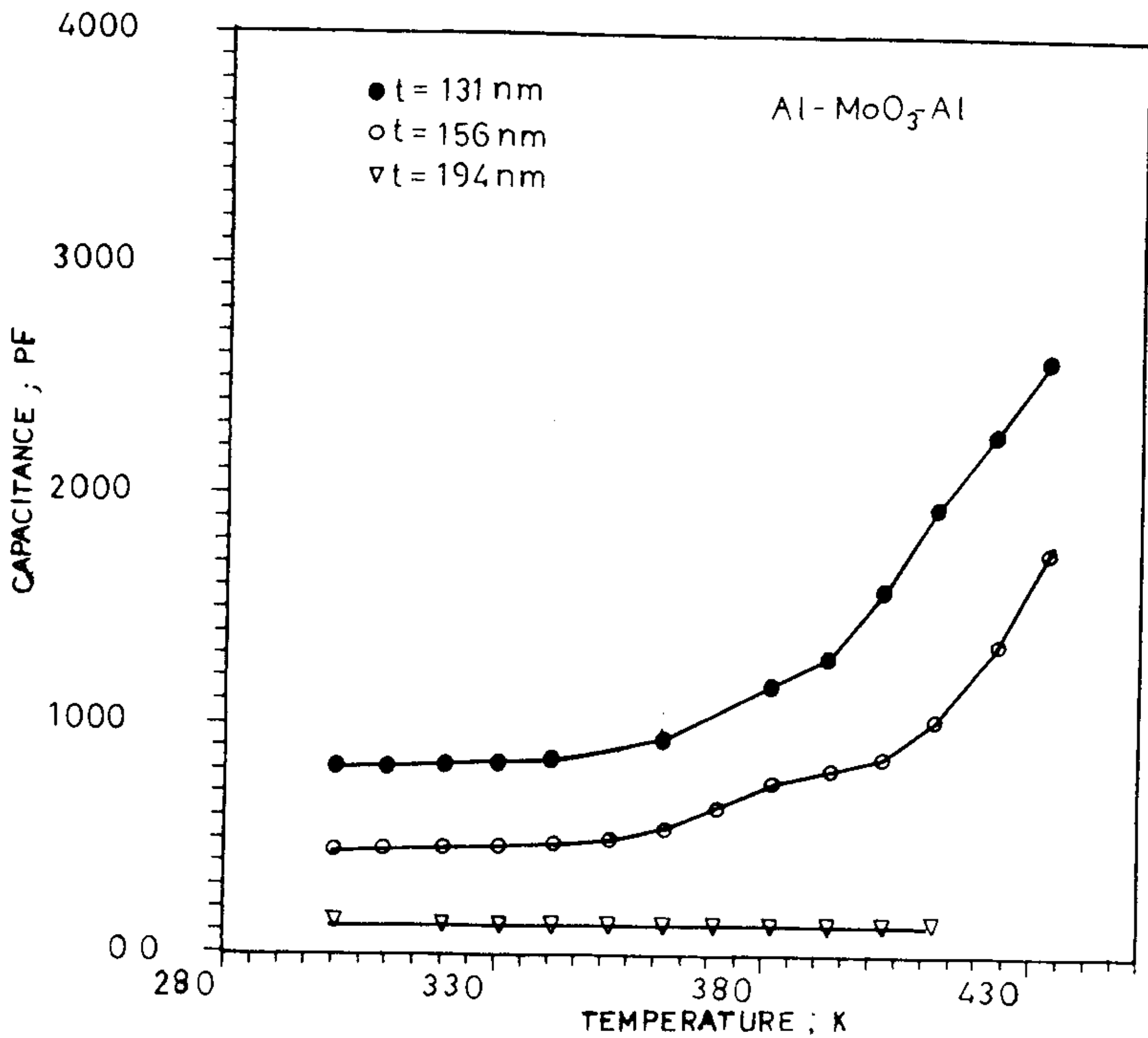

Fig.3.22. Plot of capacitance vs. temperature for Al-MoO_3-Al with MoO_3 thicknesses = 131nm, 156nm and 194 nm.

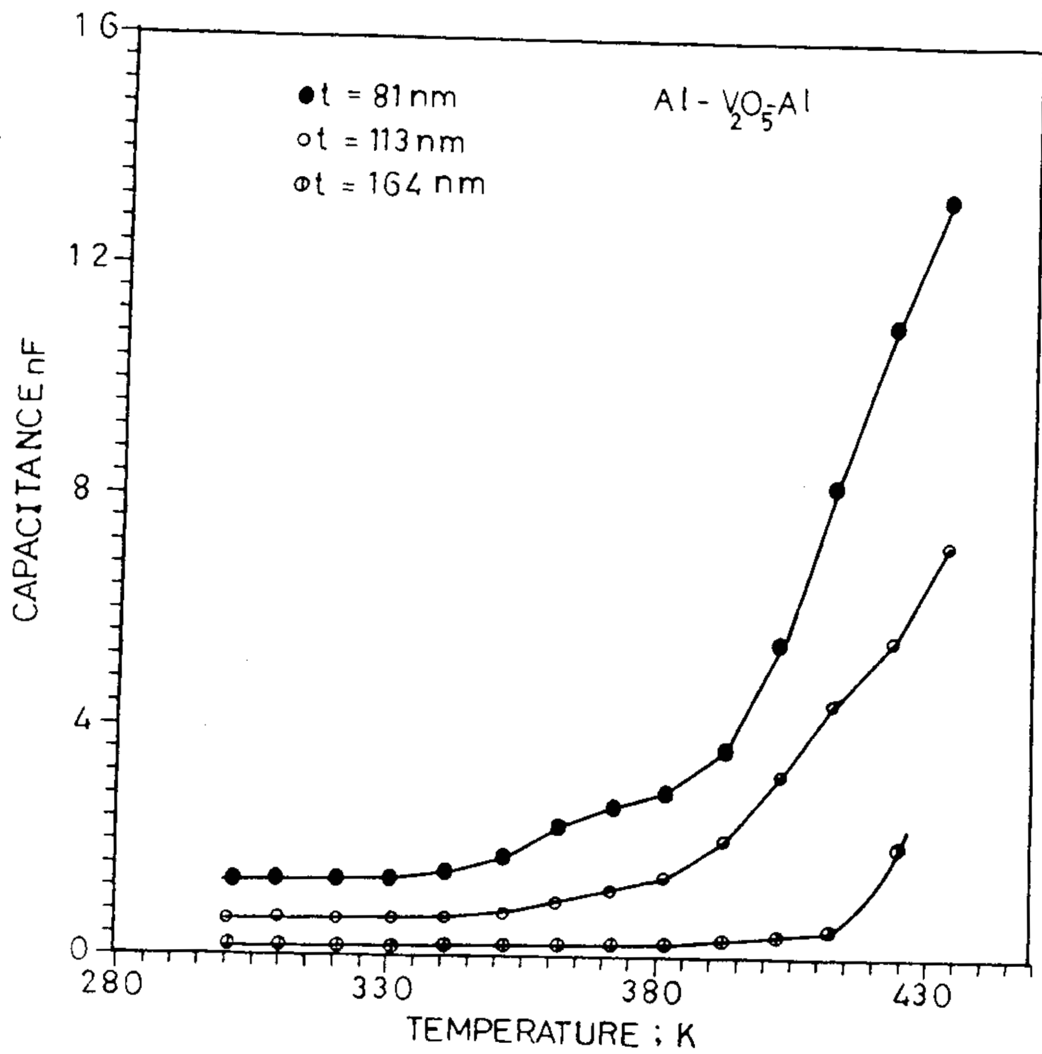

Fig.3.23. Plot of capacitance vs. temperature for $Al-V_2O_5-Al$ with V_2O_5 thicknesses = 81nm, 113nm, and 164nm

temperature.

Figure 3.24 gives the variation of capacitance of Al-TiO_2-Al with TiO_2 thicknesses 60, 111, and 153 nm. The variation becomes much faster from 410K onwards. It has been observed that as the thickness of the sandwich film decreases the capcitance increases.

In all the cases the trend in the variation of capacitance with thickness is similar. A similar variation of capacitance was reported for europium oxide (Eu_2O_3) [30].

Plot of capacitance vs inverse of MoO_3 thickness of Al-MoO_3-Al sample at room temperature are shown in figure 3.25. Figure 3.26 gives the variation of capacitance with inverse of thickness for V_2O_5 films in Al-V_2O_5-Al samples. The variation of capacitance with inverse of thickness of TiO_2 films in Al-TiO_2-Al samples are given in figure 3.27. In all the three cases straight line curves are obtained.

The logarithmic current-voltage characteristics of Al-MoO_3-Al structure with MoO_3 thicknesses 156,181,&

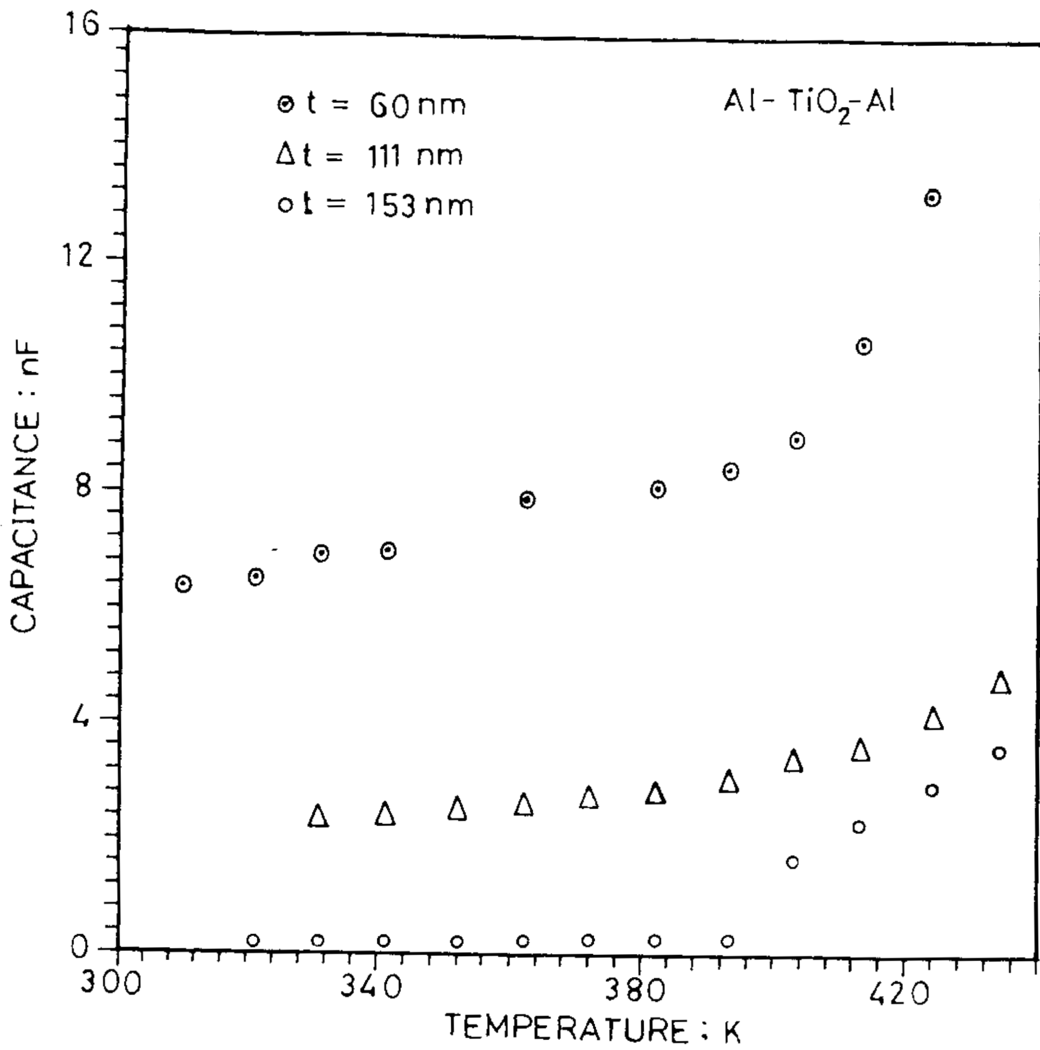

Fig.3.24. Plot of capacitance vs. temperature for $Al-TiO_2-Al$ with TiO_2 thicknesses = 60nm, 111nm, and 153nm.

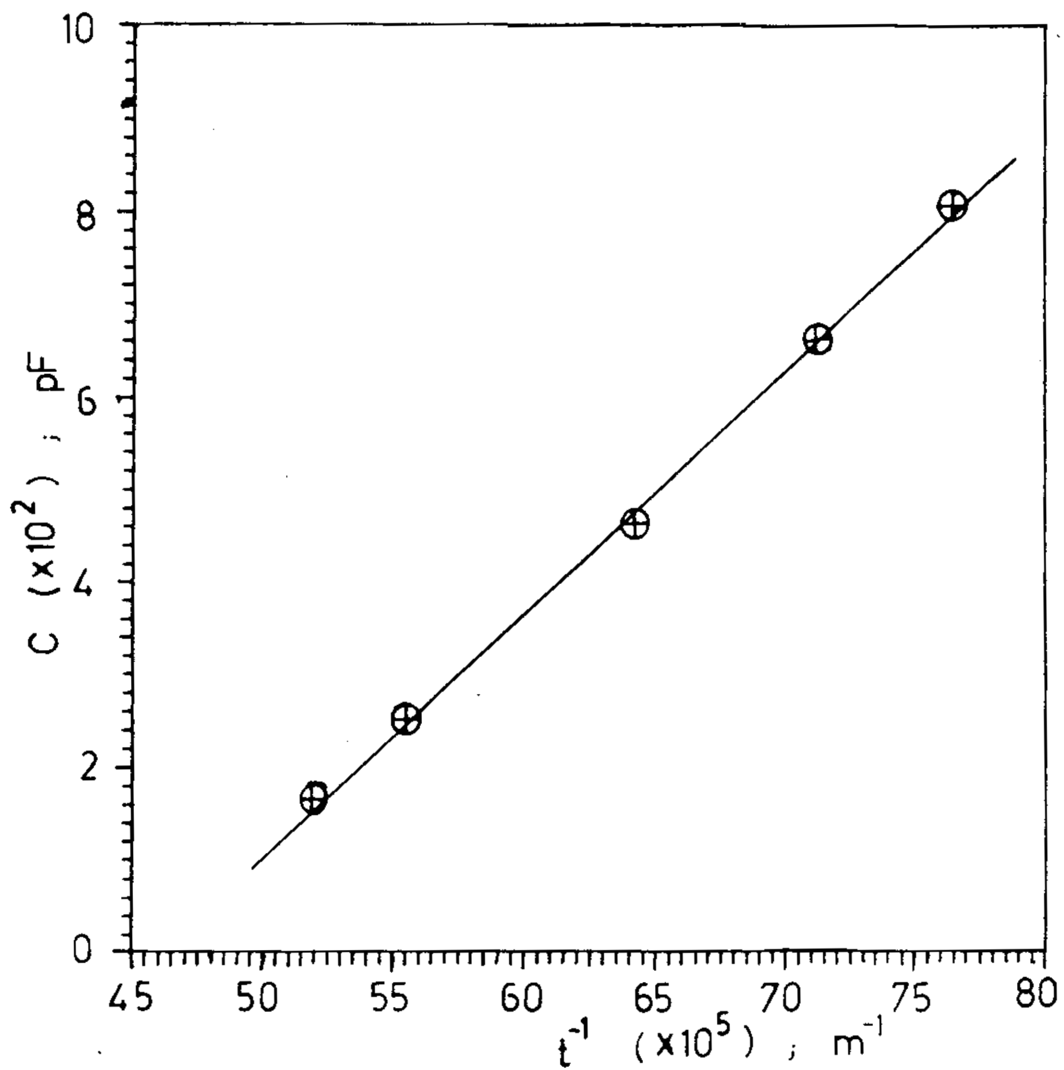

Fig.3.25. Plot of capacitance vs. inverse of thicknesses for MoO_3 film.

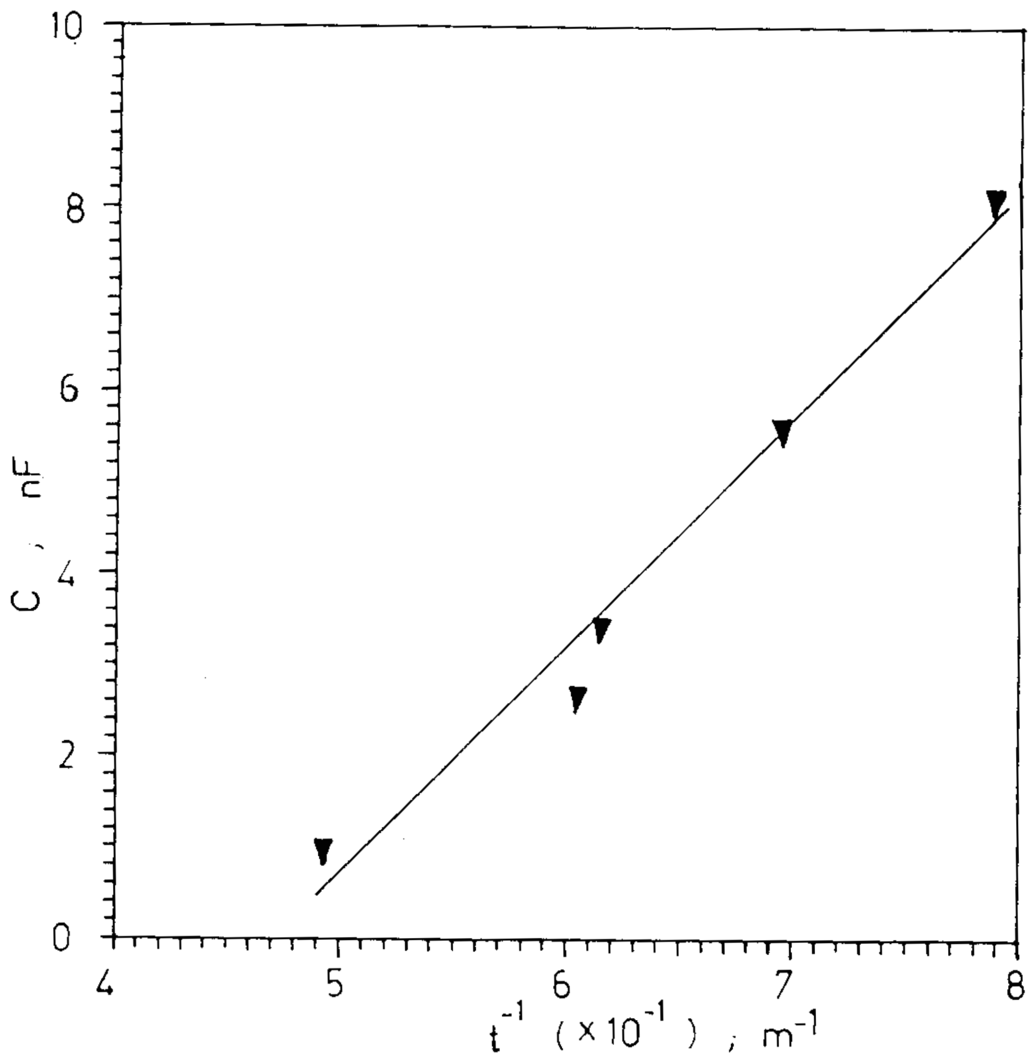

Fig.3.26. Plot of capacitance vs inverse of thickness for V_2O_5 film.

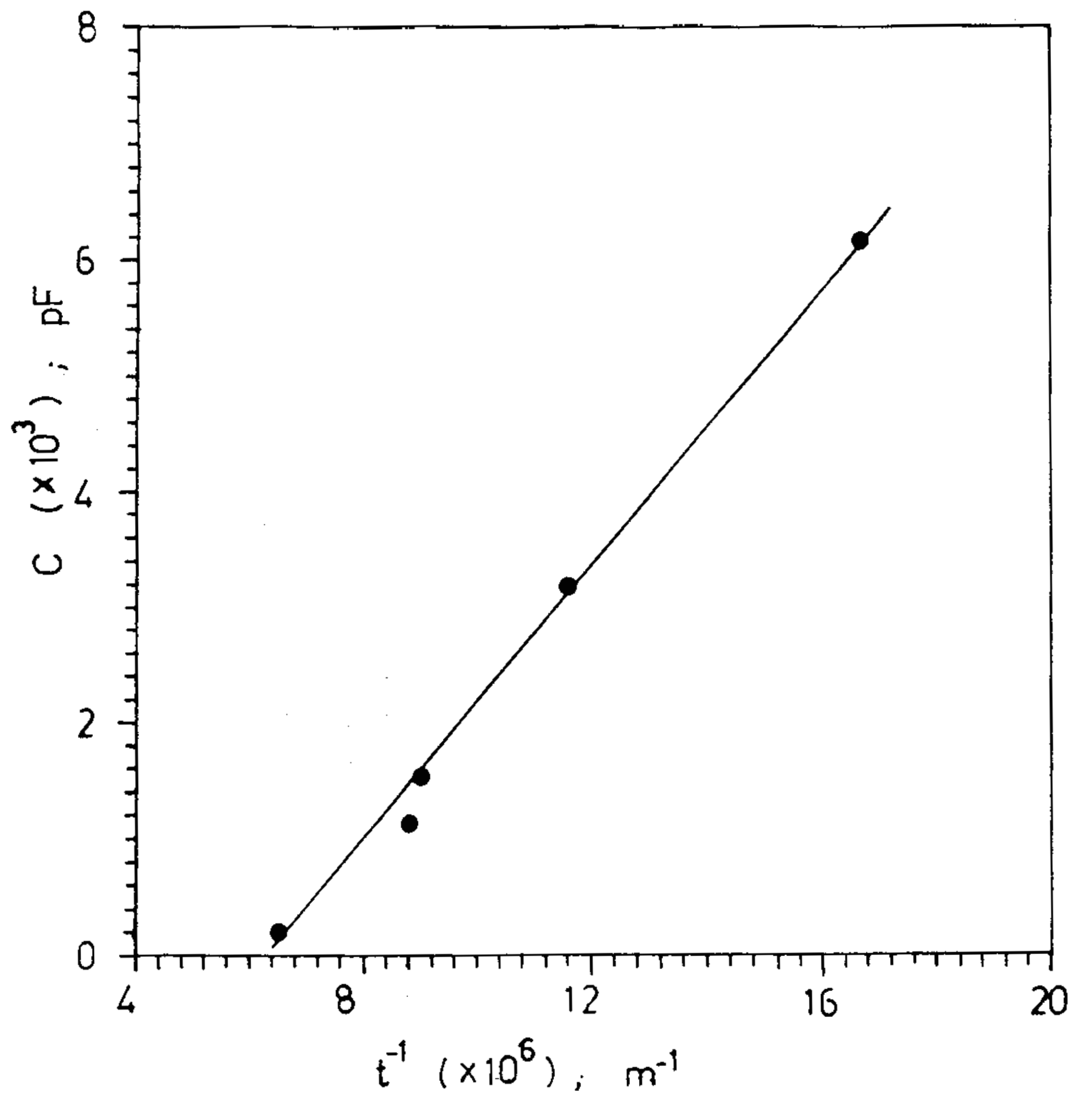

Fig.3.27. Plot of capacitance vs. inverse of thickness for TiO_2 film.

194 nm are given in figure 3.28. Figure 3.29 gives the log plot of current- voltage characteristics of Al-V_2O_5-Al with V_2O_5 thicknesses 81, 113, 127 & 162 nm. Figure 3.30 shows the log plot of current- voltage characteristics of Al-TiO_2-Al with TiO_2 thicknesses 60, 111 & 153 nm. The current I exhibits a voltage V dependence of the form $I \propto V^n$ where n depends on the field region[31]. In the cases of MoO_3 and TiO_2 some portion of the curves are linear, ie. n = 1. But in the case of V_2O_5 the nature of the curve fits the relation $I \propto V^2$. The value of n is low (n = 1) for moderate fields and it reaches up to 6 at high fields.

3.4. Conclusion

The activation energy of MoO_3, V_2O_5, and TiO_2 films are found to vary with thickness of films. DC electrical conductivity in coplanar geometry ($\sigma_{\parallel}$) and sandwich geometry ($\sigma_{\perp}$) have been measured and found that $\sigma_{\parallel}$ is much higher than $\sigma_{\perp}$ for these materials at the same temperature. Field dependent conduction mechanism in sandwich form of MoO_3 and TiO_2 films are Poole-Frenkel type. But in the case of sandwich of V_2O_5 film,

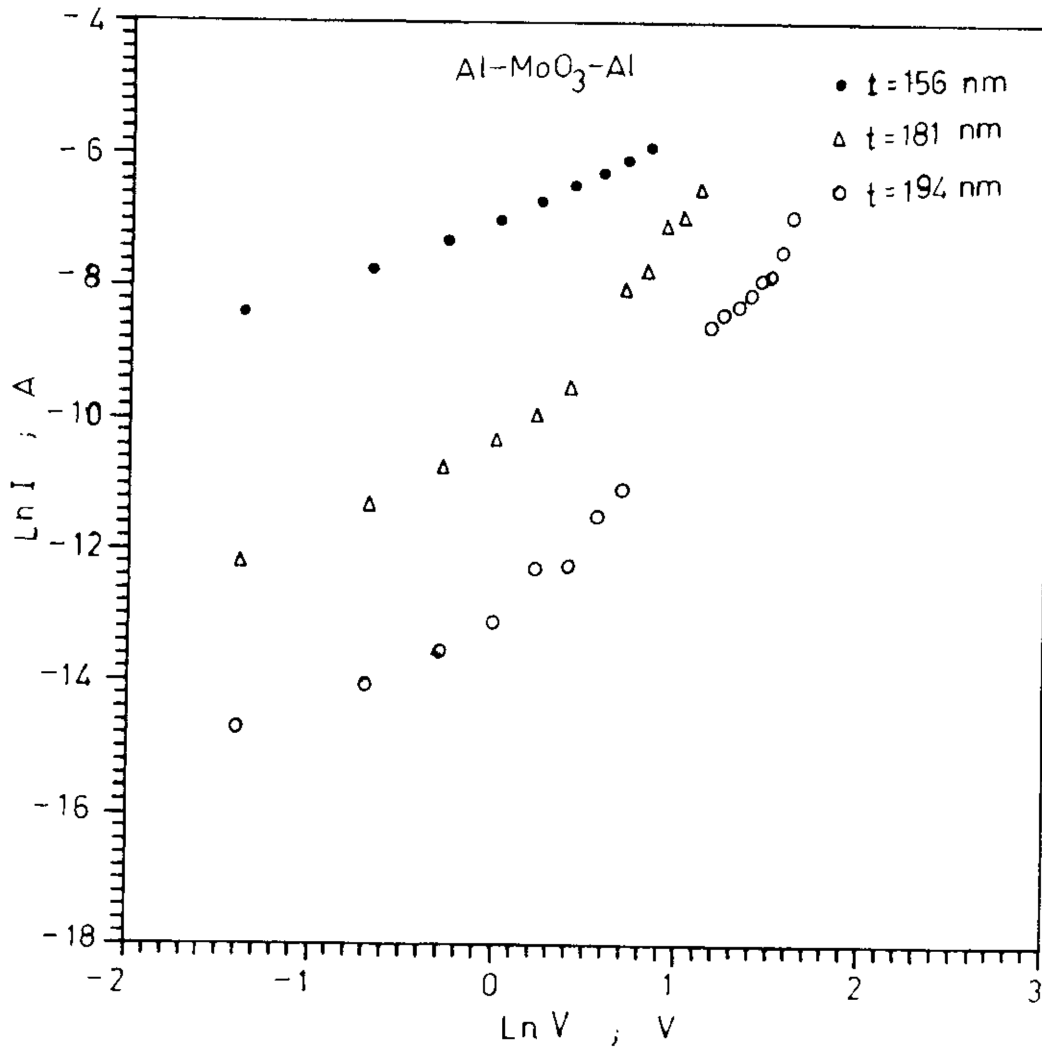

Fig.3.28. Plot of ln I vs. ln V for Al-MoO_3-Al films with MoO_3 thicknesses 156nm, 181nm & 194nm.

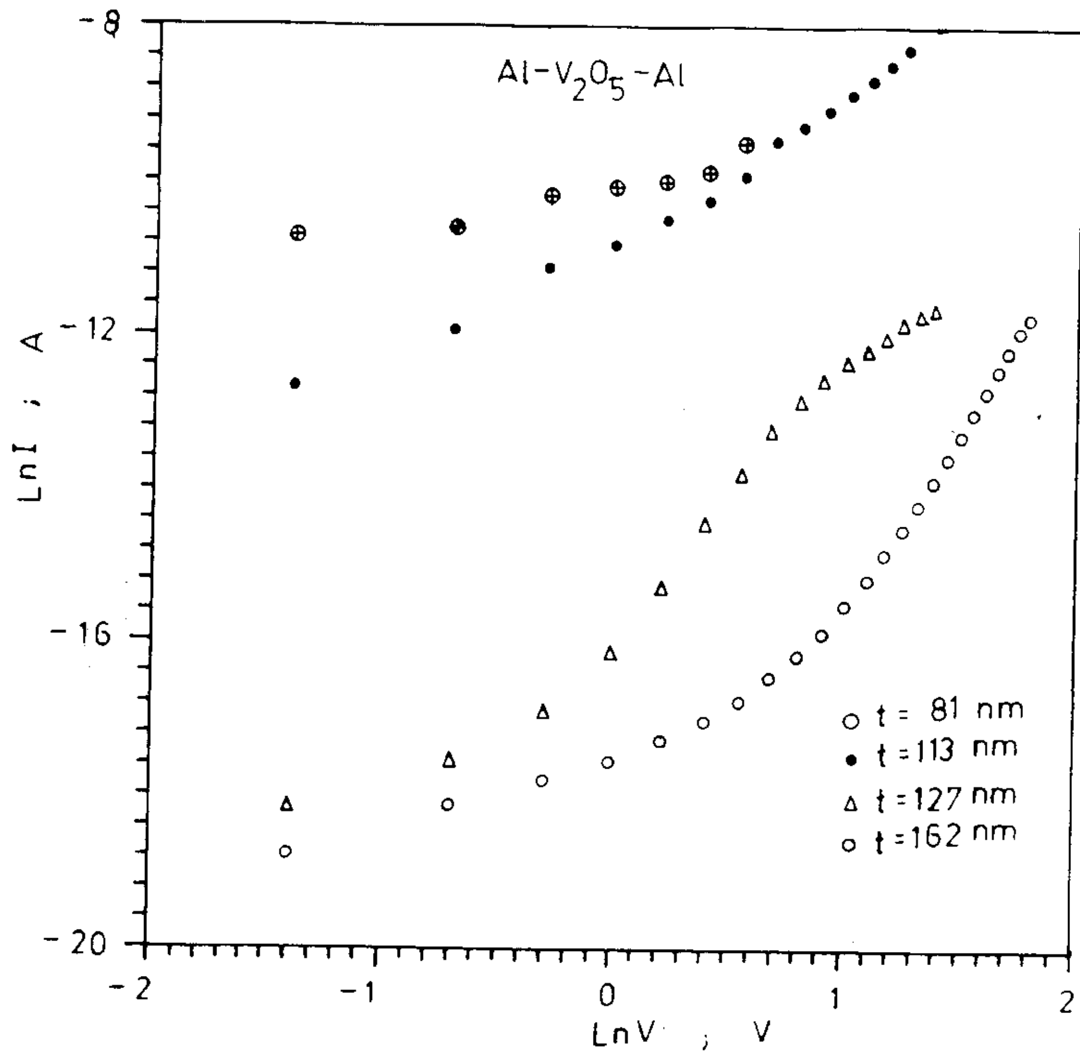

Fig.3.29. Plot of lnI with lnV for Al-V_2O_5-Al film of V_2O_5 thicknesses. 81nm, 113nm, 127nm, and 162nm.

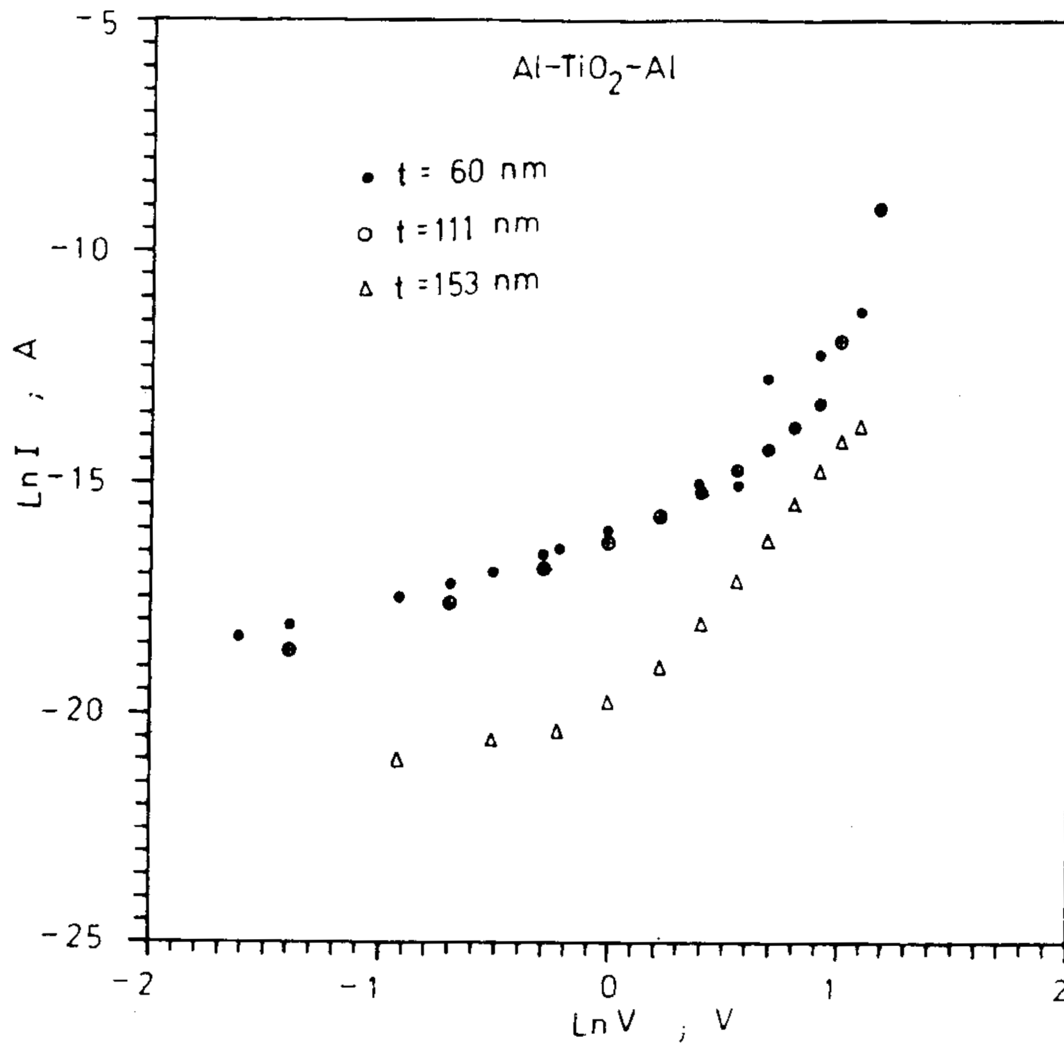

Fig.3.30. Plot of lnI with lnV for Al-TiO_2-Al film of TiO_2 thicknesses 60nm, 111nm ,and 153nm.

at high field the conduction mechanism is Poole-Frenkel type and at low field it is Schottky type. Capacitance of Al-MoO_3-Al, Al-V_2O_5-Al, and Al-TiO_2-Al are found to increase with temperature. Variation of capacitance with inverse of thicknesses of the materials gives linear plots.

References

1. E.P. Denton, H. Rawson, and J.E. Stanworth, Nature 173(1954) 1030.

2. G.A. Libowitz, Progress in solid State chemistry, Ed. H. Reiss, Vol:2, 1965,p.216 Pergamon press.

3. S.K. Deb and J.A. Chopoorian, J. Appl. Phys. 37(1966) 4818.

4. G. Anderson and A. Magneli, Acta Chemica Scandinavica, 4(1950) 793

5. M. Rapos and J.H. Calderwood, J. Phys. D 13(1975) 1838

6. M. Rapos and J.H. Calderwood, J. Phys. D 8(1975) 299

7. M. Anwar and C.A. Hogarth, Int. J. Electronics, 66(1989) 419

8. I.G. Austin and N.F. Mott, Adv. Phys. 18(1969) 41

9. T.N. Kennedy, R. Hakim, and J.D. Mackenzie, Mater. Res. Bull. 2(1967) 193

10. T. Allerrsma, R. Hakim, and T.N. Kennedy, and J.D. Mackenzie, J. Chem. Phys. 46(1967) 154

11. V.A. Ioffe and I.B. Patrina, Phys. Stat. Sol.(b), 40(970) 389

12. J. Haemers, E. Baetens, and J. Vennick, Phys. Stat. Sol. (a), 20(1973) 381

13. H.G. Bachmann, F.R. Ahmed, and W.H. Barnes, Z. Krist. 115(1961) 110

14. F.J. Morin, Bell. System Tech. J. 37(1958) 1047

15. H.N. Bogomolov, E.K. Kudinov, D.N. Mirlin and Yu.A. Firsov, Sov. Phys. Sold State 9(1968) 1630

16. V.N. Bogomolov, E.K. Kuninov, D.N. Mirlin, and Yu.A. Firsov, Sov. Phys. Solid State, 9(1968)2502

17. Nicoloso, Ber. Bunsenges. Phys. Chem. 94(1990) 731

18. G.A. Khan and C.A. Hogarth, J. Mater. Sci. 25(1990) 5014

19. P.W. Anderson, Phys. Rev. 109(1958) 1492.

20. N.F. Mott, J. Non-cryst. Solids 1(1968) 1.

21. J. Bullot, O. Gallais, M. Gauthier, and J. Livage, Appl. Phys. Lett. 36(1980) 986.

22. J. Bullot, P. Cordier, O. Gallais, M. Gauthier and J. Livage, J. Non-cryst. Solids, 68(1984) 123.

23. J.J. Legendre and J. Livage, J. Coll. Interf. Sci. 94(1983) 75

24. V.S. Pankajakshan, K. Neelakandan, and C.S. Menon, Thin Solid Films 215(1992) 196

25. P.A. Walley, Thin Solid Films, 2 (1968) 213.

26. D.K. Jain and J.C. Garg, Ind. J. Pure and Appl. Phys., 17 (1979) 642.

27. M. Anwar and C.A. Hogarth, Ind. J. Electronics 67 (1989) 551.

28. M. Anwar amd C.A. Hogarth, J. Mater. Sci. 25 (1990) 1789.

29. R.D. Gould and J.C. Bowler, Thin Solid Films, 164 (1988) 281.

30. M.K. Jayaraj and C.P.G.Vallabhan, Thin Solid Films, 177 (1989) 59.

31. R. Ramanujan, M. Radhakrishnan and C. Balasubramanian, J. Vac. Sci. Technol., A. 3 (1985) 2320.